

FOR FURTHER TRAN

St. H.
sett
12

AD A 054591

NSWC/WOL TR 77-59

**BOUNDARY-LAYER TRANSITION
EXPERIMENTS ON SHARP, SLENDER
CONES IN SUPERSONIC FREEFLIGHT**

BY DANIEL C. REDA

ADVANCED WEAPONS DEPARTMENT

30 SEPTEMBER 1977

AD No. _____
DDC FILE COPY

DDC
RECEIVED
JUN 1 1978
JY F

Approved for public release, distribution unlimited.



NAVAL SURFACE WEAPONS CENTER

Dahlgren, Virginia 22448 • Silver Spring, Maryland 20910

UNCLASSIFIED

SECURITY CLASSIFICATION OF THIS PAGE (When Data Entered)

REPORT DOCUMENTATION PAGE		READ INSTRUCTIONS BEFORE COMPLETING FORM
1. REPORT NUMBER	2. GOVT ACCESSION NO.	3. RECIPIENT'S CATALOG NUMBER
14 NSWC/WOL/TR-77-59		
4. TITLE (and Subtitle)		5. TYPE OF REPORT & PERIOD COVERED
6 Boundary-Layer Transition Experiments on Sharp Slender Cones in Supersonic Freeflight.		Final: 7/75 - 9/77
		6. PERFORMING ORG. REPORT NUMBER
		8. CONTRACT OR GRANT NUMBER(s)
7. AUTHOR(s)	9. Final rept. Jul 75 - Sep 77	
10 Daniel C./Reda		
9. PERFORMING ORGANIZATION NAME AND ADDRESS		10. PROGRAM ELEMENT, PROJECT, TASK AREA & WORK UNIT NUMBERS
Naval Surface Weapons Center White Oak Laboratory Silver Spring, Maryland 20910		61153N; WR02302; WR02302003; WA8201
11. CONTROLLING OFFICE NAME AND ADDRESS		12. REPORT DATE
		17 30 Sep 1977
		13. NUMBER OF PAGES
		67 (127 pp.)
14. MONITORING AGENCY NAME & ADDRESS (if different from Controlling Office)		15. SECURITY CLASS. (of this report)
16 WR02302		UNCLASSIFIED
17 WR02302003		15a. DECLASSIFICATION/DOWNGRADING SCHEDULE
16. DISTRIBUTION STATEMENT (of this Report)		
Approved for public release; distribution unlimited.		
17. DISTRIBUTION STATEMENT (of the abstract entered in Block 20, if different from Report)		
18. SUPPLEMENTARY NOTES		
Funding supplied by Naval Air Systems Command, Washington, D. C. 20360 (Code NAVAIR - 320C, W. C. Volz) and Naval Sea Systems Command, Washington, D. C. 20362 (Code NAVSEA 03513, L. Pasiuk).		
19. KEY WORDS (Continue on reverse side if necessary and identify by block number)		
Boundary-layer transition Wall-temperature-ratio Unit-Reynolds-number effects Transition-zone asymmetry		
20. ABSTRACT (Continue on reverse side if necessary and identify by block number)		
Transition experiments were conducted on sharp, slender ($\theta_c = 5^\circ$) cones, at $M_\infty = 4.5$, in an aeroballistics range. Data acquisition was accomplished with dual-plane spark shadowgraphs. Wall-to-adiabatic wall temperature ratio was varied from $\approx .2$ to $\approx .5$ by cryogenically cooling the range gas, at two distinct edge unit Reynolds numbers, $(U_e/v_e) = 0.94$ and $2.82 \times 10^6/\text{in.}$ Unit-Reynolds-number influence on transition and transition zone asymmetry (TZA) as a function of non-dimensional angle of attack (α/θ_c) were also		

DDC
 REPRODUCED
 JUN 1 1978
 ALBUQUERQUE
 F

391 596

JOB

UNCLASSIFIED

SECURITY CLASSIFICATION OF THIS PAGE(When Data Entered)

investigated. Transition reversals with increased wall cooling were noted at both (U_e/v_e) values. A strong unit-Reynolds-number influence on transition was observed for $(U_e/v_e) > \approx 10^6/\text{in}$, substantiating results of Potter. Comparisons of present TZA data with the empirical model of Potter and with other $M_\infty \approx 5$ data showed that transition contours, at $(\alpha/\theta_c) > 0$, may not be adequately described by a singular dependence on (α/θ_c) .

UNCLASSIFIED

SECURITY CLASSIFICATION OF THIS PAGE(When Data Entered)

SUMMARY

Boundary-layer transition experiments were conducted on sharp, slender cones in an aeroballistics range as part of the coordinated program for transition research recommended by the U.S. Transition Study Group. The present report documents all phases of this research program.

This research was jointly sponsored by the Naval Air Systems Command, Mr. William C. Volz (AIR-320C), monitor, and the Naval Sea Systems Command, Mr. Lionel Pasiuk (SEA-03513), monitor.

Because the references in this report are numerous, they have been listed in a reference list at the back rather than footnoted on the page where first cited. Microfilm readers are encouraged to make a print of this list to refer to while reading the report.

Ralph A. Niemann

R. A. NIEMANN
By direction

ACCESSION for	
N°IS	Re Section <input checked="" type="checkbox"/>
DDC	Buff Section <input type="checkbox"/>
UNANNOUNCED	<input type="checkbox"/>
JUSTIFICATION	
BY	
DISTRIBUTION/AVAILABILITY CODES	
Dist.	
<i>A</i>	

CONTENTS

	<u>Page</u>
I. INTRODUCTION	1
II. DEFINITION OF TEST ENVIRONMENTS	3
III. EXPERIMENTAL APPARATUS AND TEST TECHNIQUES	5
A. Ballistics Range Facility	5
B. Environmental Chamber	6
C. Model	8
IV. DATA REDUCTION PROCEDURES	12
V. RESULTS	15
A. Wall-Temperature-Ratio Results	15
B. Unit-Reynolds-Number Effects	18
C. Transition-Zone-Asymmetry Results	20
VI. CONCLUSIONS	24
REFERENCES	57
LIST OF SYMBOLS	62

ILLUSTRATIONS

<u>Figure</u>	<u>Title</u>	<u>Page</u>
1	Definition of Test Conditions; Velocity and Temperature	26
2	Definition of Test Conditions; Pressure	27
3	Range Schematic	28
4	Photograph of Launcher	29
5	Photograph of Model and Sabot	30
6	Photograph of Environmental Chamber	31
7	Internal Schematic of Environmental Chamber	32
8	Thermal Calibration of Chamber; Horizontal Temperature Distributions	33
9	Thermal Calibration of Chamber; Vertical Temperature Distributions	34
10	Thermal Calibration of Chamber; Transient Response	34
11	Model Schematic	35
12	Transition Run Length vs. Time of Flight for Three Most Severe Heating Trajectories	36
13	Bluntness Effects	37
14	Spark Shadowgraph; All Laminar Flow	38
15	Spark Shadowgraph; Transitional Flow	39
16	Transition Zone Asymmetry Due to Angle of Attack, as Reported by Potter	40
17	Transition Reynolds Number vs. Wall-to-Adiabatic Wall Temperature Ratio; Present Data	43
18	Transition Reynolds Number vs. Wall-to-Adiabatic Wall Temperature Ratio; Present Data vs. Potter and Sheetz	44
19	Transition Reynolds Number vs. Wall-to-Adiabatic Wall Temperature Ratio; Present Data vs. Stetson and Krogmann	45
20	Transition Reynolds Number vs. Unit Reynolds Number; Present Data vs. Potter and Sheetz	46
21	Transition Reynolds Number vs. Unit Reynolds Number; Present Data vs. Krogmann and Stetson	47
22	Transition Zone Asymmetry; (a-h) Present Data vs. Potter Curves	48-51
23	Transition Zone Asymmetry; Comparisons with Other Mach Five Data, $.35 < (\alpha/\theta_c) < .50$	52
24	Transition Zone Asymmetry; Comparisons with Other Mach Five Data, $.15 < (\alpha/\theta_c) < .25$	53
25	Transition Zone Asymmetry Due to Angle of Attack; Potter versus Krogmann	54
26	Transition Reynolds Number versus Wall-to-Adiabatic Wall Temperature Ratio; Sensitivity to Corrections	55
27	Transition Reynolds Number versus Unit Reynolds Number; Sensitivity to Corrections	56

TABLES

<u>Table</u>	<u>Title</u>	<u>Page</u>
1	Summary of Primary-Ray Data	41
2	Average Values and Maximum Variability of Test Parameters	42

I. INTRODUCTION

Boundary-layer transition, aside from being one of the classical unsolved problems of basic fluid physics, remains a real-world problem to designers of advanced flight systems. Accurate predictions of viscous flow fields around high-speed aircraft, missiles, and re-entry vehicles are of paramount importance to each system's design and subsequent flight performance. Boundary-layer transition is known to significantly affect vehicle dynamics, drag, and surface heat-transfer rates. To date, universally valid empirical and/or semiempirical correlations for boundary-layer transition onset, location, and degree of symmetry (or asymmetry), as a function of one or more of the many variables which influence it, have been lacking. The great reservoir of experimental data obtained under wind-tunnel conditions has recently come under critical scrutiny due to findings which demonstrated that facility noise can dominate or seriously compromise transition results.^{1,2} These facts, and many other pertinent, unanswered questions concerning this phenomenon, have been documented in the detailed surveys of Tani³, Morkovin⁴⁻⁷, and Reshotko⁸.

Due to the critical nature of this problem area to both DOD and NASA, there evolved at the beginning of the present decade a national committee, the U.S. Transition Study Group (USTSG). Its objectives were "to develop and implement a program that would do something constructive toward resolving the many observed anomalies in boundary-layer transition data and that might provide some basis for future estimation of transition Reynolds numbers. The group formulated specific experimental programs emphasizing careful and redundant measurements, documentation of the disturbance environment, and elimination, wherever possible, of facility induced transition." NASA, Navy, Air Force, and other government laboratories active in transition research were asked to send representatives and to actively participate towards attaining the stated technical goals. Dr. Eli Reshotko of Case Western Reserve University was named Chairman; his recent paper⁹ summarizes the Committee's recommended research program. Progress has been made on several fronts, as witnessed by the six papers following Reference 9 (i.e., AIAA Journal, Vol. 13, No. 3, March 1975, pp. 266-314).

The "pre-committee" research of Sheetz 10-14, at the Naval Ordnance Laboratory, and of Potter¹⁵, at the Arnold Engineering and Development Center, had demonstrated the utility of ballistics ranges for boundary-layer transition research. This capability for conducting transition experiments in quiescent environments resulted in the Committee's formulation of additional research tasks to be conducted at both Laboratories⁹.

The Arnold Center was to focus on unit Reynolds number effects, while also conducting a series of sensitivity studies on various test-related factors which might influence transition in ballistics-range environments. This research was conducted by Dr. J. L. Potter and was reported in References 16 and 17.

The Naval Ordnance Laboratory was to focus on wall-temperature-ratio effects on transition. During the first five years of USTSG's existence, the NOL portion of this overall program was not conducted, due to a lack of funding for four years, and, in the other year, a lack of facility time despite availability of funding.

In 1974, the Naval Ordnance Laboratory became part of the newly-formed Naval Surface Weapons Center. In 1975, Dr. W. C. Lyons, Jr., the original NOL representative to the USTSG, was reassigned to a high-level managerial position within NSWC and this author was appointed to USTSG as his replacement. A research effort based on USTSG recommendations was formulated in 1975 and jointly funded during the FY 76/TQ/FY 77 period by the Naval Air Systems Command and the Naval Sea Systems Command.

The objective of this research was to experimentally investigate the influence of wall-to-adiabatic wall temperature ratio on smooth-wall boundary-layer transition in supersonic free flight. In addition to this primary objective, an independent check on the unit Reynolds number phenomenon, as observed by Potter in the A.E.D.C. ballistic range, was to be made. Experimental results concerning both these questions were obtained, along with information concerning boundary-layer transition zone asymmetry due to small angles of attack. These results are presented herein as the Naval Ordnance Laboratory's contribution to the USTSG's research program.

At the completion of testing in December, 1976, all ballistics range facilities at NSWC were closed.

II. DEFINITION OF TEST ENVIRONMENTS

Inviscid calculations were undertaken in order to define free flight test environments wherein $(T_w/T_{aw})_e$ could be varied over a finite regime as the independent variable, while holding both M_e and (U_e/v_e) fixed. A sharp, slender ($\theta_c = 5^\circ$) cone geometry was selected as consistent with the nature of USTSG objectives and compatible with testing in a ballistics range facility.

For the short flight times encountered in such facilities, cone surface temperature (T_w) remains essentially constant at its initial value ($\approx 540^\circ R$), except in the immediate vicinity of the cone tip (this topic will be discussed in more detail in subsequent sections). Variations in $(T_w/T_{aw})_e$ are thus accomplished through variations in the recovery, or adiabatic-wall, temperature of the flow. For a sharp cone at zero incidence:

$$(T_{aw})_e = T_e \left[1 + r \left(\frac{\gamma - 1}{2} \right) M_e^2 \right] \quad (1)$$

where $r = \text{constant}$ (here 0.9) and

$$\frac{T_e}{T_\infty} = \frac{\left[1 + \left(\frac{\gamma - 1}{2} \right) M_\infty^2 \right]}{\left[1 + \left(\frac{\gamma - 1}{2} \right) M_e^2 \right]} \quad (2)$$

Thus, for a given cone geometry, at a given M_∞ , $(T_{aw})_e$ varies in direct proportion to T_∞ , the static temperature of the range gas.

A test technique was thereby defined, wherein T_∞ would be independently varied to achieve the desired variations in $(T_w/T_{aw})_e$. In order to ensure a constant flight Mach number, cone launch velocity would be properly chosen to match each T_∞ level ($M_\infty = U_\infty/C_\infty$, with $C_\infty \propto \sqrt{T_\infty}$). Further, P_∞ would be independently set for each flight to ensure a constant edge unit Reynolds number (U_e/v_e). Figures 1 and 2 show results of such calculations in the regime $.2 \leq (T_w/T_{aw})_e \leq .6$ for a 5° half-angle cone at $M_\infty = 4.5$ ($M_e = 4.27$), for $(U_e/v_e) = 9.33$ and $29.56 \times 10^5/\text{inch}$, for flights in nitrogen.

It will be noted that absolute values of (U_e/ν_e) chosen here are higher than those recommended in Reference 9. The P_∞ regime of $\approx .1$ to 1.0 atm. was defined, on the low end, by requirements to maintain sufficient freestream density to yield high-quality spark-shadowgraph records of the boundary-layer flow, and, further, to ensure transition on the cone surface; pressures above 1.0 atm. would have complicated the facility modifications and test procedures for this program and were not pursued.

Secondary test objectives were to be met by conducting a series of $M_\infty = 4.5$ flights at room temperature conditions, $(T_w/T_{aw})_e = 0.21$, with variations in (U_e/ν_e) being accomplished through variations in freestream static pressure.

Two additional parameters, Re_L and (U_e^2/ν_e) are discussed here, as pertinent to both the temperature-ratio and unit-Reynolds-number tests.

Cone length was constant for all tests conducted. Therefore, for the temperature-ratio tests, $Re_L = (U_e/\nu_e) \cdot L_c$ was constant; (U_e^2/ν_e) could not be maintained constant, however, due to variations in U_∞ , and thus U_e , for tests at constant Me and (U_e/ν_e) . (Maximum variability of all test parameters will be discussed in Section V.)

For the unit-Reynolds-number tests, Re_L increased in direct proportion to (U_e/ν_e) due to use of a constant length cone. An alternative approach would have been to decrease L_c as (U_e/ν_e) was increased, thereby maintaining Re_L constant. Such additional experiments have been proposed, and, if conducted, may well yield some understanding of the unit-Reynolds-number phenomenon (i.e., does the forward or upstream progression of a transition zone with increasing Reynolds number depend on the percentage of total vehicle surface area already covered by turbulent flow, and, is the mechanism for this "upstream influence" associated with the propagation of self-radiated noise through the subsonic portions of the laminar boundary layer?). Variations in (U_e^2/ν_e) during the unit-Reynolds-number tests occurred also, in direct proportion to variations in (U_e/ν_e) .

Details of how these test environments were created, and how the tests were conducted, are discussed in the following section.

III. EXPERIMENTAL APPARATUS AND TEST TECHNIQUES

A. BALLISTICS RANGE FACILITY

All tests were conducted in the Naval Surface Weapons Center/White Oak Laboratory 300-foot Pressurized Ballistics Range (PBR). A simplified schematic is shown in Figure 3. Principal components of this facility will be discussed briefly, in the sequence they occur along the model flight path. Subsections B and C will provide more detailed information concerning the environmental chamber and the model.

All models were launched from a single-stage, powder-driven, smooth-bore (76/40) gun, 1.625" I.D. nominal. A photograph of this launcher is shown in Figure 4. The model/sabot package, shown in Figure 5, incorporated the hollow-base/bore-size model design used by Potter^{16,17}; in this design, propellant gases act on the model directly, and are contained by a lexan seal ring at the model base. The smooth launcher bore allowed all models to be launched without spin.

Once the package clears the muzzle, it is exposed to the static pressure environment within the blast tank. Here, the sabot, comprised of four separate/inter-locking lexan fingers, is aerodynamically stripped from the model. The model traverses the blast tank and enters the range tube through a 4" I.D. entrance pipe, while the sabot sections diverge from the model flight path due to aerodynamic lift and are destroyed on impact with a series of metal "witness" plates.

In the present program, the blast tank was always operated at the same static pressure level as the range tube, thereby avoiding any flow of the test gas between range compartments. The rubber-bellows coupling between blast tank and range tube served to acoustically isolate the walls of the range tube from disturbances propagated through the blast tank bulkhead due to sabot impact. Further, since the model always traveled supersonically relative to the freestream, it outran all acoustic disturbances propagated through the test gas due to gun blast.

A series of electronic timing devices and single-spark/split-beam shadowgraph optics, were used to define the model's trajectory and angle of attack history within the range tube, both uprange and down range of the environmental chamber.

Figure 6 shows a photograph of the environmental chamber, a 21-foot long, 5-foot diameter compartment within which the various (Tw/Taw)e environments were created. Its entrance was located 146'3" from the gun muzzle, sufficiently distant to isolate its interior from light and blast wave contaminants associated with launch.

Reference 18 provides a state-of-the-art summary of ballistics-range technology, as it existed at the start of this decade, for those desiring additional information.

B. ENVIRONMENTAL CHAMBER

Figure 7 schematically shows internal details of the environmental chamber. Its primary purpose was to create various test environments by establishing uniform - temperature-level regions of gas ($\approx 200. < T_{\infty} < 540. ^\circ R$) through which the conical models could be flown. A series of cryogenic-coil panels were mounted on the external surfaces of a wood-frame structure, centered about the flight-path axis. This coil-support structure was itself supported within a metal cylinder, or inner bulkhead. All voids between the coil-support structure and the inner bulkhead and between the inner and outer bulkhead (range-tube walls) were filled with thermal insulation. Pin-supported, collapsable, thermal barriers were positioned over the model entrance and exit holes to complete the thermal containment of the test gas within the chamber.

Three pairs of spark-source/single-pass shadowgraphs were used to optically record flowfields about the free flight models within the chamber. These shadowgraph stations were located $3\frac{1}{2}$ feet apart, centered on the longitudinal axis of the chamber; each pair was arranged in a dual-plane mode so as to provide simultaneous perpendicular views of the model. Spark firing was properly sequenced for each station based on signals from a proportional-timer/delay-circuit, whose inputs were defined by measured model traversal times between two light-screen stations located immediately uprange of the chamber entrance. Spark firing times were 0.2 μ sec. in duration.

A 14" x 24" sheet of Kodack Tri-X Ortho film was positioned on the lower internal surface of the coil-support structure directly across from each spark source and held flat by a protective overlay of optical glass. This film was selected for its compatibility with spark intensity/duration and excellent resolution over the entire temperature regime experienced.

Two survey wires were strung through the chamber, positioned left and right of range center, so as to cut across the outer limit of each optical path, thereby providing a reference line for true horizontal on exposed film sheets, from which model orientation could be determined.

Test environments were created in the following manner. After the model/sabot package was loaded into the gun, and film sheets were positioned in the environmental chamber, the entire range facility was sealed and evacuated to a pressure level of ≈ 1 mm Hg, absolute. This served to remove all air and associated moisture. Liquid nitrogen, stored in a cryogenic tank located outside the range building, was pumped to a manifold adjacent to the environmental chamber, then circulated through the coils internal to the chamber. Spray nozzles were located at several positions along these internal coolant lines and were remotely activated from outside the chamber. This arrangement allowed for a portion of the liquid nitrogen to be expanded and vaporized within the chamber, providing dry nitrogen as the test gas itself, as well as providing additional cooling via the liquid-to-gas phase change. Liquid nitrogen not used in this manner was vented outside the chamber.

By properly controlling liquid nitrogen flow rates through the coils and nozzles, required static temperature and pressure levels within the chamber could be achieved. The remainder of the range tube external to the chamber was also filled with dry gaseous nitrogen at room temperature, at the same static pressure level maintained within the chamber.

A procedure was established whereby the volume of test gas within the chamber was always cooled below the desired static temperature, at a pressure level slightly above that required for a given shot. Liquid nitrogen circulation was then terminated and gaseous nitrogen within the chamber was allowed to settle for approximately 15 to 20 minutes while T_{∞} approached the desired level from below. During actual testing, centerline static temperatures were monitored by a series of retractable thermocouples. Once the desired uniform temperature level was achieved within the chamber, the static pressure level was adjusted, via suction, to match the desired test condition, thermocouples were withdrawn, the thermal barriers were dropped, and the gun fired. Model traversal of the test chamber was always complete within two seconds after the signal was given to drop the thermal barriers.

Figures 8 and 9 show static temperature distributions measured by a fixed array of thermocouples during thermal calibration of the environmental chamber. Horizontal centerline distributions, for all temperature levels, were found to be quite uniform, particularly within the data acquisition region of the chamber. Some nonuniformities were noted in the vertical

centerline distributions for the lowest temperature levels utilized, but variations across the maximum flight-path core (+2." from range centerline) were always within $\approx 10\%$ of centerline values; variations of $(T_w/T_\infty)_e$ between the four photographed model rays were, for any given flight, considerably less since boundary-layer-edge streamlines originated from static gas which passed through the model shock wave in the immediate vicinity of the cone tip.

Figure 10 shows transient thermal response data also obtained during initial thermal calibration of the chamber. The main point here is that the volume of test gas was sufficiently large, and the shadowgraph stations were sufficiently removed from the chamber ends, such that no appreciable rise in the static temperature level occurred prior to model passage.

Noise measurements were also made within the chamber using a 1/8" D. Bruel and Kjaer condenser microphone. This instrument was similar to that utilized by Potter^{16,17} but with an expanded frequency range (5 Hz to 160 K Hz). Signals from this instrument, both amplified and unamplified, were recorded on a multi-channel tape recorder during several firing sequences. Results are summarized below.

Freestream static pressure fluctuations of $\approx 6.4 \times 10^{-4}$ mm Hg abs., peak-to-valley, were measured. For a minimum freestream static pressure level of 76. mm Hg abs, $(\delta/p_\infty)_{\max} \approx 8.4 \times 10^{-6}$, peak-to-valley; this corresponds to an rms range for $(\delta/p_\infty)_{\max}$ from 2.1 to 2.8×10^{-6} , essentially identical to that reported by Potter^{16,17}. Such levels are three to four orders of magnitude below levels associated with wind-tunnel facilities¹⁹.

Noise associated with the falling of the two thermal barriers was measured and found to decay to background levels within 0.7 seconds after its inception. No noise above the stated background level was recorded between this event and model passage.

C. MODEL

Figure 11 shows a schematic of the model, which, as noted previously, was based on model designs used by Potter^{16,17}. This model also possessed the same basic external geometry as the one used by Dougherty^{2,20} in his studies of transition in a wide variety of wind-tunnel facilities. (Under USTSG guidance, a joint AEDC/NASA flight-test program will be conducted during FY 78 at the NASA Dryden Flight Research Center, wherein this same 50° half-angle cone geometry will be boom-mounted ahead of an F-15 aircraft and flown over a wide Mach number/altitude regime; transition data so generated should prove most interesting in comparison with both ballistics-range and wind-tunnel results).

Each model was fabricated from an integral piece of titanium, and, as a result, possessed no surface discontinuities. Internal ballast was used to provide a relatively high static margin (11.3%), required for stability in free flight.

Potter^{16,17} investigated various features of ballistics-range testing which might influence transition results measured in such facilities: model vibrations, surface roughness, non-uniform surface temperature distributions, and angle-of-attack. In summary of Potter's sensitivity studies, none of the first three model-related factors was found to compromise his reported transition results; further, his findings concerning these factors can justifiably be applied to present experiments, conducted at similar test conditions, wherein such sensitivity studies were outside the scope of the recommended NOL program⁹. Model surface roughness and surface thermal effects will be discussed below, however, as they relate to the present model design and environments to which these models were subjected. Effects of nose bluntness on departures from the sharp-cone flow regime will also be discussed, as pertinent to present test conditions. Discussions of angle-of-attack effects will be deferred until Sections IV and V.

1. SURFACE ROUGHNESS AND WAVINESS. Model surface roughness and waviness were measured with a Taylor-Hobson "Talysurf" profilometer possessing a stylus tip of .0001" radius. Measurements were made on four of the twenty-two models fabricated. Traces were obtained on each of two rays, both near the cone mid-point and near the model base. Maximum surface roughness values ranged from 5.8 to 8.3 μ - inches, rms; since peak-to-valley roughness heights can be approximated by (4 x rms), maximum peak-to-valley dimensions were \approx 23 to 33 μ - inches. Surface waviness was measured at .00006 to .00018 inches maximum amplitude, peak-to-valley, with wavelengths ranging from 0.22 to 0.35 inches, peak-to-peak, which translates into amplitude-to-wavelength ratios of \approx .0003 to .0005. Internal sabot surfaces in contact with the model were machined to surface roughness finishes of 28 μ -inches, rms, or better.

Admittedly, surface roughness measurements with a stylus whose tip radius is approximately three times the maximum peak-to-valley roughness dimension being traversed is not precise. However, Potter's sensitivity study showed that surface roughness of \approx 300 μ -inches rms (\approx 1200. μ -inches, peak-to-valley) were required before measured transition locations, at $M_\infty = 5.$, $(T_w/T_a)_e = .19$, were influenced. Such roughness dimensions are accurately measureable with profilometer techniques. Further, all present experiments were conducted at wall-temperature ratios above those of Potter, which translates into relatively thicker boundary layers and thus even less sensitivity to surface roughness.

Prior to launch, the external surface of each model was cleaned with pure grain alcohol, which served to remove any possible surface deposits and which, upon evaporation, left no residue of its own.

2. SURFACE THERMAL EFFECTS. Surface thermal effects which might influence boundary-layer transition data obtained in a ballistics range are: nonuniform wall-temperature distributions, tip to afterbody; tip melting or ablation; and time variations of the afterbody temperature level itself.

Potter^{16,17} conducted an analysis concerning possible hot-tip effects on boundary-layer transition for slender cones at Mach five, based on the work of Rhudy²¹. His conclusions were that nonuniform temperature distributions, resulting from differential aerodynamic heating of the model tip versus model afterbody, were "not an obvious factor" on transition data measured under stated test conditions. Further, since present models were fabricated from titanium, with a melt temperature of $\approx 3200^{\circ}\text{R}$, tip melting was not possible (maximum stagnation temperature for present experiments was $\approx 2570^{\circ}$ to 2730°R , depending on whether or not real gas effects are accounted for).

The third point listed above concerns increases in T_w with time, and whether or not such increases were sufficient to alter the stability of the laminar boundary layer over the duration of any given flight. Based on methods of References 22-24, calculations of $T_w(t)$ were made for the most severe heating trajectory experienced ($U_{\infty} = 5200$ ft/sec, $P_{\infty} = 1$ atm, $T_{\infty} = 540^{\circ}\text{R}$). In-depth thermal conduction was modeled in a one-dimensional sense. Results for this case showed a maximum ΔT_w of $\approx 40^{\circ}\text{R}$ during flight from muzzle exit to environmental chamber, corresponding to $\approx 7\%$ increase (.215 to .23) in the primary independent variable (T_w/T_{aw})_e. Thermal penetration depths were found to be less than the model wall thickness, justifying the one-dimensional assumption. Such maximum variations in the primary independent variable during any flight were not sufficient to alter trends observed, and conclusions reached, during the present program. Figure 12 adds experimental credence to this statement. Measured transition run lengths, for the three most severe heating trajectories flown, are shown as a function of flight time. Combined range-tube and environmental-chamber data for these room-temperature shots demonstrates that no consistent increasing, or decreasing, trend in X_{TR} , as a function of time, was observed.

3. BLUNTNESS EFFECTS. Present models were machined to a hemispherically-blunt tip, .005" in radius, identical to the value utilized by Potter^{16,17}. Each model was viewed with an optical comparator to ensure that such nosetip specifications were met.

It is a well established fact that small amounts of tip bluntness significantly influence transition behavior on slender cones at supersonic and hypersonic speeds (e.g., the work of Stetson and Rushton²⁵). In the "small-bluntness regime," as nosetip radius is increased, transition is observed to move rearward. Further, the degree of rearward movement has been shown to correlate with the entropy-swallowing distance, i.e., that wetted length which must be traversed by the laminar boundary layer before it entrains essentially all mass which passed through the blunt (non-conical) portions of the model bow shock.

For a given blunt-cone geometry at a given freestream Mach number, it has been shown²⁶ that all flowfields become self-similar when viewed in terms of the non-dimensional parameter \bar{S} , where

$$\bar{S} = \left(S/R_N \right) \left(Re_{N,t} \right)^{-1/3} \quad (3)$$

and,

$$Re_{N,t} = \left(\frac{\rho c}{\mu} \right)_t \cdot R_N \quad (4)$$

i.e., variations of boundary-layer edge conditions along the cone surface are defined by a single curve for all combinations of nose radius and Reynolds number. In the regime $1 < \bar{S} < 10$, for $\theta_c = 5^\circ$, edge conditions vary rapidly as the flow adjusts from blunt-body conditions to sharp cone limits; it is in this regime that essentially all entropy swallowing occurs.

To ensure that boundary-layer transition would occur, for test conditions of present interest, solely within the sharp-cone regime, a series of calculations was made using eqs. (3) and (4), to define the downstream limit ($\bar{S} = 10$) of the entropy swallowing region as a function of nosetip radius. Results are shown in Figure 13. In all cases, for $R_N = .005"$, entropy swallowing was calculated to be complete within $\approx 1.0"$ of the tip, while measured X_{TR} values were always $\approx 2.5"$.

IV. DATA REDUCTION PROCEDURES

As noted earlier, dual-plane spark-shadowgraph stations were used to provide simultaneous, perpendicular views of the model flow field, yielding transition data on each of four conical rays, located every 90° around the body. Examples of photographs obtained in this manner are shown in Figures 14 and 15. In Figure 14, the entire body is covered with laminar flow, with transition occurring in the recompression region of the near wake. In Figure 15, transition occurs on the body near its mid-point.

Transition location, X_{TR} , was defined (and read) as that run length along each conical ray to the station where breakdown to turbulence was complete, i.e., downstream of this location, no further regions of intermittent laminar flow were observed. This definition of X_{TR} corresponds to locations near the middle-to-end of a transition zone as defined by conventional surface heat-transfer and/or surface pitot-probe techniques²⁷. It should be further noted that shadowgraphs provide an instantaneous record of a basically unsteady flow phenomenon and that a distribution of X_{TR} values is expected, even for nominally steady-flow conditions (e.g., Figure 3 of Reference 27). Data scatter associated with such a measurement technique is best illustrated in Section V, wherein all results of the present effort will be presented.

Perpendicular views of the model silhouette at each station allows the total model angle of attack, the plane in which it occurs, and the circumferential orientation of each photographed ray relative to the true windward ray, to be determined. Measured in-plane angles of attack, α_H and α_V , were converted²⁸ to total model angle of attack, and ray orientation angles relative to true windward, in the following manner: (Note that "horizontal" and "vertical" are arbitrary designations for range-left and range-right views; recall Figure 7)

$$\alpha = \left(\alpha_H^2 + \alpha_V^2 \right)^{1/2} \quad (5)$$

$$\phi' = \tan^{-1} \left(\frac{\alpha_H}{\alpha_V} \right) \quad (6)$$

$$\phi_{V, \text{ wind}} = \phi' \quad (7)$$

$$\phi_{V, \text{ lee}} = 180^\circ - \phi' \quad (8)$$

$$\phi_{H, \text{ wind}} = 90^\circ - \phi' \quad (9)$$

$$\phi_{H, \text{ lee}} = 90^\circ + \phi' \quad (10)$$

Since $\alpha_H \geq \alpha_V$, $0^\circ \leq \phi' \leq 90^\circ$, and the primary ray, or ray closest to true windward, is defined by the smaller of $\phi_{V, \text{ wind}}$ and $\phi_{H, \text{ wind}}$; the primary ray always possesses a ϕ value $< 45^\circ$.

Having defined an X_{TR} value on the primary ray, it remains to correct this measured value for angle of attack effects. Figure 16 presents the set of curves used by Potter^{16,17} for this purpose. These curves give a description of transition-zone asymmetry on sharp, slender cones as a function of non-dimensional angle of attack (α/θ_c) and are based on transition zone location data, measured via shadowgraph and/or surface heat-transfer techniques, in the wind-tunnel experiments of Ward²⁹, DiCristina³⁰, and Mateer³¹. Implicit in this figure is the assumption that, while noise, unit Reynolds number, wall-temperature ratio, etc. influence transition zone location on a cone at zero incidence, once this run length (X_{TR} , $\alpha = 0^\circ$) is determined for any particular set of test conditions, then the

development of transition zone asymmetry with increasing angle of attack is solely a function of (α/θ_C) . As noted in Figure 16, corrections to present primary-ray data ($\phi < 45^\circ$), for $\phi > 0^\circ$, $\alpha > 0^\circ$, were obtained by linear interpolation between the $\phi = 0^\circ$ and $\phi = 60^\circ$ curves, $0 < (\alpha/\theta_C) \leq .6$, and, as a result, were generally small. (Sensitivity of present results to the correction procedure used will be discussed in Section V, C.)

All boundary-layer edge parameters were calculated for a sharp cone at zero incidence, assuming ideal-gas relations ($\gamma = 1.4$; gas constant for N_2 of $1776 \text{ ft}^2/\text{sec}^2\text{-OR}$), and a laminar-flow recovery factor of 0.9. Viscosity for nitrogen was calculated, based on Sutherland's law, by

$$\mu_e = 7.042 \times 10^{-7} \left[\frac{(T_e)^{1.5}}{(T_e + 198.6)} \right], \text{ # m/ft-sec} \quad (11)$$

V. RESULTS

During the present program, 22 models were fabricated, 20 were successfully launched into the range tube, and 18 of these flights yielded acceptable primary-ray data ($\alpha/\theta_c \leq .60$ at shadowgraph stations within the environmental chamber). Table I summarizes all primary-ray data, subdivided into three sequential sets: wall-temperature-ratio data at high (u_e/v_e); wall-temperature-ratio data at low (u_e/v_e); and unit-Reynolds-number data. Repeatability of results is demonstrated by shots 6717 and 6720. Table II summarizes average values and maximum variability of principal test parameters, as achieved.

Subsections A, B, and C present plots and discussions of wall-temperature-ratio data, unit-Reynolds-number data and transition-zone-asymmetry data, respectively. Selected comparisons with existing data will also be shown. (Initial comparisons of these results with data presented at the AGARD Symposium on Laminar-Turbulent Transition, May, 1977, were made by this author³² serving in the role of commentator.)

A. WALL-TEMPERATURE-RATIO RESULTS

Effects of wall cooling on stability and transition of compressible laminar boundary layers have been investigated in a significant number of wind-tunnel experiments, with widely varying results being documented (e.g., Figure 1 of Richards and Stollery³³ and Figure 3 of Morkovin⁶).

Based on theoretical work of Lees and Reshotko³⁴, Reshotko³⁵, and Mack³⁶, Reshotko³⁷ discussed effects of wall cooling on the stabilization of 1st and 2nd mode disturbances. He noted, in concurrence with Reference 33, that observed differences in transition behavior with wall cooling could not be explained by differing measurement techniques, but rather were a result of differing dominating frequencies in the disturbance spectra associated with the various facilities utilized. Further, depending on the (U_e^2/v_e) regime, variations in $(T_w/T_{aw})_e$ could have a differing influence on stabilization of the various disturbance modes; the higher the value of (U_e^2/v_e), the less the importance of the higher modes, and the more likely that a given disturbance frequency would

correspond to the lowest mode. Transition reversals with increased cooling could thus be reasonably expected based on linear stability arguments.

Mack³⁸ recently applied linear stability theory in an attempt to explain wall-cooling effects on transition in the presence of various wind-tunnel-generated disturbance spectra; cooling in the $(T_w/T_{aw})_e$ regime from 1.0 to 0.7, at $Me = 2.7$, was noted to be stabilizing, in agreement with reported data of Van Driest and Blumer³⁹ and Van Driest and Boison⁴⁰. Extension to very cold walls was not attempted.

The only controlled, ground-based experiments into wall-cooling effects on transition, in the absence of radiated noise and freestream turbulence, are those ballistics-range experiments of Sheetz^{11,13} and the present effort. Such free flight experiments have an advantage associated with data acquisition in truly quiescent environments. However, by their very nature, barring significant breakthroughs in physical integrity and cost of telemetry-type instrumentation, such experiments are limited to macroscopic observations of the phenomenon in question. The exact nature of transition - promoting disturbances and how they are amplified by the laminar boundary layer, leading to its eventual breakdown to turbulence, cannot be ascertained from range testing alone. Detailed microscopic experiments such as those conducted by Kendall⁴¹, are a necessary complement to this work as called for in the USTSG recommended program for transition research⁹.

Figure 17 shows a plot of transition Reynolds number versus wall-to-adiabatic wall temperature ratio, for each of two distinct edge unit Reynolds numbers, as measured during the present experiment. At high unit Reynolds number ($2.8 \times 10^6/in$) transition data were obtained over the $(T_w/T_{aw})_e$ regime from .51 to .23; cooling was noted to be destabilizing from .51 to $\approx .35$, and stabilizing from $\approx .35$ to .23. At low unit Reynolds number ($0.94 \times 10^6/in$), transition data were obtained over a slightly less-expanded $(T_w/T_{aw})_e$ regime, from .45 to .22; here, no established trend was noted with cooling from .45 to $\approx .3$, whereas a definite stabilizing influence was evident from $\approx .3$ to .22, just as in the higher unit Reynolds number case.

A destabilizing influence (decreasing Re_{TR}), followed by a stabilizing influence (increasing Re_{TR}), is here referred to as a "transition reversal". If one speculates on the functional dependence of Re_{TR} on $(T_w/T_{aw})_e$ from 1.0 to $\approx .5$ (the maximum value of the present experiment), based, say, on results of References 38, 39 and 40, then this observed behavior might also be referred to as a "transition re-reversal". The potential for multiple-reversals must be acknowledged, based on the gun-tunnel/flat-plate transition results of Richards and Stollery³³ and the shock-tube/wall-boundary-layer transition studies of Boison⁴².

Reversals in Re_{TR} with cooling also tend to further discount any plausible arguments concerning surface roughness effects on transition under present test conditions; since the laminar boundary layer tends to thin with increased cooling, surface roughness, if a dominant factor, would tend to further decrease observed transition Reynolds numbers, counter to observed behavior.

Figures 18 and 19 show comparisons of present results with data from four other sources: Potter^{16,17}, Sheetz¹³, Stetson²⁵ and Krogmann⁴³. In all cases, transition measurements were made on sharp, slender cones in the edge Mach number regime from four to five.

In Figure 18, comparisons are made solely with other ballistics-range data. Sheetz¹³ varied the wall temperature ratio by use of an environmental chamber, employing a test procedure similar to the one used here; in Reference 13, data at $(T_w/T_w)_e < .2$, for $M_\infty \approx 5$, were obtained by heating the volume of test gas above room temperature. Potter's^{16,17} two values of $(T_w/T_w)_e$ resulted solely from the fact that tests were conducted at two different Mach numbers, with $T_\infty \approx 540^\circ R$. Two points are noted here. First, Potter's $Me=4.3$ and 2.1 data are seen to be in nominal agreement with transition Reynolds numbers measured here. The collapse of his two separate Mach number data sets in transition-Reynolds-number versus unit-Reynolds-number coordinates may be due to the fact that these data sets apparently bracket a region of transition reversal. Second, Sheetz's observation of a transition reversal at colder-wall conditions than those of the present experiment represents another demonstration of the potential for multiple reversals of Re_{TR} with wall cooling (recall References 33 and 42).

In Figure 19, comparisons are made with two data sets obtained in facilities other than conventional wind tunnels: the shock-tunnel results of Stetson²⁵ and the Ludwig - tube results of Krogmann⁴³. Wall-temperature-ratio variations were accomplished, in the first case, through variations in shock strength and, in the second case, through variations in reservoir total temperature. These data sets provide interesting comparisons for two reasons: first, maximum (U_e/v_e) and (U_e^2/v_e) values for these experiments are of the same order as minimum values experienced in the present effort; second, although not documented, disturbance environments associated with these two facility types may be significantly different from those experienced in conventional/long-run-time wind tunnels (along these lines, no unit-Reynolds-number influence on transition was observed in either facility, as will be illustrated in the next subsection).

Krogmann⁴³ found no dependence of Re_{TR} on wall cooling in the regime $.98 > (Tw/Taw)e > .5$. Stetson's²⁵ data showed a definite destabilizing influence (decreasing Re_{TR}) as $(Tw/Taw)e$ was varied from $\approx .5$ to $\approx .2$, at which point a slight indication of a stabilizing influence (or possible reversal) was noted. Considering the nearly identical Me , (U_e/ve) and (U_e^2/ve) values of these two experiments, it is perhaps more than coincidental that the resulting data sets merge, in good agreement with one another, at their point of overlap, $(Tw/Taw)e \approx .5$.

Transition Reynolds numbers measured at low (U_e/ve) in the present experiment were noted to be in good quantitative agreement with values measured by Stetson, in the wall-temperature-ratio regime $\approx .45$ to $\approx .3$. Trends with increased cooling, however, were noted to be somewhat different, with a transition reversal clearly indicated at $(Tw/Taw)e \approx .3$ in the present case, versus a possible reversal at $\approx .2$ in the Stetson experiment.

B. UNIT-REYNOLDS-NUMBER EFFECTS

Technical background concerning this most perplexing issue is well summarized in the discussions of Reshotko^{8,37} and the most recent reviews of Whitfield and Dougherty²⁰ and Morkovin⁷. Reshotko^{8,37} presented a mathematical argument based on dimensional analysis and linear stability theory which dictates a power-law dependence between transition Reynolds number and either a non-dimensional frequency proportional to (U_e^2/ve) , or a non-dimensional wavelength proportional to (U_e/ve) , depending on whether the disturbance spectrum is best characterized by a physical frequency or wavelength. Whitfield and Dougherty²⁰, reiterating and extending the work of Pate and Schueler¹, further demonstrated that acoustic disturbances, radiated by turbulent wall boundary layers, play a dominant role on boundary-layer transition as measured in wind-tunnel facilities. Since such disturbances scale with unit Reynolds number, at least a partial explanation for this phenomenon as observed in wind-tunnel experiments, has been afforded. Morkovin⁷ has stated that the unit-Reynolds-number effect on transition is more likely attributable to a combined response of the laminar boundary layer to a superposition of several or more (usually unknown) disturbance factors; a single, unique dependence of transition Reynolds number on unit Reynolds number should not, therefore, be expected.

Figure 20 shows a plot of transition Reynolds number versus unit Reynolds number; present data are shown in comparison with the ballistics-range data of Potter^{16,17} and Sheetz¹³. Except for the addition of Potter's Mach two data, all results were obtained for $Me \approx 4.5$ and $(Tw/Taw)e \approx .2$. In all cases, unit-Reynolds-number variations were obtained through variations

in the freestream static pressure level, at constant freestream velocity and static temperature ($\approx 540^{\circ}\text{R}$). The dimensional frequency ($Ue^2/\nu e$) thus varied proportionately with unit Reynolds number.

Within the unit-Reynolds-number range ≈ 1.5 to $\approx 3.0 \times 10^6/\text{inch}$, present data were found to support the strong unit-Reynolds-number influence on transition observed by Potter. A least-squares fit of present results in this stated regime, for Re_{TR} proportional to $(Ue/\nu e)^n$, yielded a value for the exponent n of 0.71, approximately ten percent above the 0.63 value dictated by the combined data sets of Potter. Since all unit-Reynolds-number tests were conducted at room temperature, supplemental shadowgraph pictures were also obtained from the split-beam stations within the range tube itself (recall Figure 12); these data, although not plotted with the primary-ray data of Figure 20, further confirmed the stated 0.71 value.

Transition Reynolds numbers measured on those two flights at unit Reynolds numbers below $10^6/\text{inch}$ were noted to be less consistent with Potter's data. During the higher unit-Reynolds-number test of these two, transition was complete only on the leeward side; indications of turbulent bursts were clearly evident on the primary ray, but they occurred too near the end of the test surface to allow a conclusive statement concerning complete breakdown to turbulence. The lowest unit-Reynolds-number flight was completely laminar on all rays, with transition being observed in the recompression region of the near wake. Therefore, while no decisive statement can be made concerning unit-Reynolds-number influence on transition in this regime, these data, when viewed versus an extension of the least-squares-fit to data above $10^6/\text{inch}$, appear to indicate a lessening ($Ue/\nu e$) influence on Re_{TR} as unit Reynolds number is decreased.

Transition Reynolds numbers measured at high and low unit Reynolds numbers, as plotted in Figure 17, were paired at nominal wall-temperature-ratio values of .30, .35, .40 and .45 and plotted in Re_{TR} versus $(Ue/\nu e)$ coordinates. The so-called unit-Reynolds-number effect was seen to persist; while no systematic dependency of the exponent n on $(T_w/T_{aw})_e$ was noted, its value remained in the 0.4 to 0.7 regime.

Figure 20 also shows transition Reynolds numbers measured by Sheetz¹³, at $(T_w/T_{aw})_e \approx .2$, as replotted from Figure 18. His data were noted to be in close quantitative agreement with both present data and Potter's results, but were too limited in scope to define any trend with unit Reynolds number, at stated test conditions. Sheetz¹⁴ did, however, conduct a limited test series wherein $(Ue/\nu e)$ was the primary independent

variable; results obtained on sharp slender cones at $Me \approx 7.$, for $\approx 10^6 < (Ue/ve) < \approx 10^7$ /inch, defined an exponent $n \approx .21$. This finding, when viewed in combination with the $Me \approx 4.5$ results, illustrates a potential Mach number influence on the phenomenon in question.

In summary, combined ballistics-range results have shown a unit-Reynolds-number influence on transition of equal or greater magnitude than found in wind-tunnel experiments. Further, the physical mechanism(s) for this influence, for flights through quiescent environments, has yet to be defined. Additional range tests at constant body-length Reynolds number (recall Section II), and flight-test experiments of the AEDC transition cone²⁰ (recall Section III, C), may well provide further insight.

Figure 21 shows a comparison of present unit-Reynolds-number data with results of Stetson²⁵ and Krogmann⁴³. In Stetson's experiment, unit-Reynolds-number variations resulted from variations in initial shock-tube static pressure and shock strength; in Krogmann's experiment, they resulted from variations in the reservoir stagnation pressure.

Krogmann observed no unit-Reynolds-number influence on transition over the wall-temperature-ratio regime .67 to .79. Similarly, if one subdivides Stetson's data into discrete sets, with $(Tw/Taw)_e = \text{constant}$, as was done in Figure 21, then the absence of any unit-Reynolds-number influence on transition in his experiment is also clearly illustrated.

As was noted in discussions concerning Figure 20, present data showed a strong unit-Reynolds-number influence on transition above $\approx 10^6$ /inch, but appeared to indicate a lessening influence as (Ue/ve) was decreased below $\approx 10^6$ /inch.

In his discussions of linear stability theory and its relationship to unit-Reynolds-number influence on transition, Reshotko³⁷ has postulated that, for a given disturbance environment, Re_{TR} is proportional to $(Ue/ve)^n$, where the exponent n may be a function of Me , $(Tw/Taw)_e$, and possibly even (Ue/ve) itself, to allow for deviations from a strict power-law dependence. Present data taken by themselves, or when viewed in comparison with lower (Ue/ve) results of Stetson and Krogmann, may provide an example of this postulated behavior, i.e., unit-Reynolds-number influence on transition depending on the unit-Reynolds-number regime experienced.

C. TRANSITION-ZONE-ASYMMETRY RESULTS

Experimental information concerning the three-dimensional, or asymmetric, nature of transition on slender bodies at angle of attack is important for two reasons. First, as discussed in

Section IV, a procedure must be available for correcting ballistics-range ($\phi > 0^\circ$, $\alpha > 0^\circ$) transition data to zero angle of attack. As noted, Figure 16 was used by Potter^{16,17}, and herein, for this purpose. Such a family of curves, by itself, provides no insight as to why transition asymmetries develop at $(\alpha/\theta_c) > 0$, rather it provides an empirical description of these asymmetries at test conditions close to those of the two ballistics range experiments under discussion.

The second reason for providing a valid model for transition-zone asymmetry stems from design requirements to accurately predict asymmetric heat-transfer distributions, and asymmetric forces/moments (both shear and induced-pressure components), on slender freeflight bodies at angle of attack. For example, the strategic-systems community has defined the importance of these requirements as they relate to predictions of frustum-transition-induced contributions to reentry-body dispersions (e.g., References 44, 45 and 46). Of course, transition-zone-asymmetry data on sharp, slender cones represent a limiting case, in that actual flight bodies always possess some finite degree of bluntness.

Having focused attention on the need for experimental information in this area, Figures 22, a-h, 23 and 24 are presented, which show comparisons of present data with Potter's curves, and comparisons of both these items with other Mach five data. Implications of these results to ballistics-range data-reduction procedures will then be reviewed. Finally, some brief comments will be offered on the apparent state-of-the-art for modeling transition-zone contours around slender vehicles at angle of attack.

Figures 22 (a-h) show comparisons of all transition run-length data measured during the present program with curves reported by Potter^{16,17}. Results are plotted in terms of non-dimensional transition run length ($X_{TR}/X_{TR, \alpha = 0^\circ}$) versus circumferential body angle ϕ , from windward (0°) to leeward (180°); non-dimensional angle of attack, (α/θ_c) , is the parameter, with data being divided into eight discrete bands, up to a maximum value of 0.63.

Since primary-ray X_{TR} values were corrected, via linear interpolation between Potter's $\phi = 0^\circ$ and 60° curves, in order to define $X_{TR, \alpha = 0^\circ}$, agreement between present data and Potter's curves is "forced" for $\phi < 45^\circ$. However, having defined $X_{TR, \alpha = 0^\circ}$ for each station of each trajectory, it was then used to non-dimensionalize measured X_{TR} values on the three non-primary rays ($45^\circ \leq \phi \leq 180^\circ$). No attempt was made here to categorize data in terms of wall-temperature ratio, unit Reynolds number, etc., consistent with the principal assumption behind Figure 16, i.e., that transition zone asymmetry on sharp, slender cones is a function

solely of (α/θ_c) . The only labeling notes the number of shots and the number of individual measurement stations which yielded data in each (α/θ_c) regime.

Several observations were made. First, at $\alpha = 0^\circ$ (Figure 22,a), present data exhibited a +20% axial variation about the nominal value of 1.0, for all circumferential locations. Such variations are a direct result of taking a finite number of "instantaneous" data samples of a basically unsteady (time-varying) flow phenomenon²⁷. As angle of attack increased (Figures 22, b-h), transition was noted to move increasingly forward on the cones leeward rays. Non-primary-ray data ($\phi \geq 45^\circ$) remained within an approximate +20 to 25% band about Potter's curves. Based on these comparisons alone, the assumption of transition-zone asymmetry depending solely on (α/θ_c) appears, to first order, to be justified.

Figures 23 and 24 show comparisons of present data and Potter's curves with other Mach-five transition-zone-asymmetry data: Krogmann⁴³, Korsia and Marcillat⁴⁷, Stetson and Rushton²⁵, and Whitfield and Dougherty²⁰ (Figure 24 only). Coordinates are those used in Figure 22.

At a non-dimensional angle of attack of ≈ 0.4 (Figure 23), all data, save the windward-ray data of Krogmann, were noted to be self-consistent. At a nominal (α/θ_c) value of ≈ 0.2 (Figure 24), fairly wide variations between the various data sets were observed.

Transition-zone asymmetry on sharp, slender cones may not, in fact, be adequately described by a singular dependence on (α/θ_c) . Flow parameters such as Mach number, wall-temperature ratio, unit Reynolds number, etc., may influence observed asymmetries; other potential sources of influence which must be considered are the disturbance environments associated with the particular facility utilized, and the measurement technique(s) incorporated. In any case, combined results of Figures 23 and 24 raise a question concerning the sensitivity of conclusions reached in Sections V, A. and B., and in References 16 and 17, to the correction procedure for $(\phi > 0^\circ, \alpha > 0^\circ)$ utilized.

A review of available data shows that Potter's windward-ray curve (faired through data of Ward²⁹) represents the minimum observed rearward movement of transition with increasing (α/θ_c) , while the windward-ray data of Krogmann⁴³ represent the maximum rearward movement observed (See Figure 25). As noted, all $(\phi > 0^\circ, \alpha > 0^\circ)$ corrections to present X_{TR} values were applied only to primary-ray data ($\phi < 45^\circ$), via linear interpolation between the $\phi = 0^\circ$ and 60° curves of Potter. It was decided to re-reduce

these data, correcting for ($\phi > 0^\circ$; $\alpha > 0^\circ$) based on linear interpolation between Krogmann's $\phi = 0^\circ$ and Potter's $\phi = 60^\circ$ curves. Primary-ray data, corrected to $\alpha = 0^\circ$ by both techniques, are shown in Figures 26 and 27.

Although absolute values for Re_{TR} were, for most flights, slightly reduced through use of Krogmann's curve, trends observed and conclusions reached in Sections V, A and B, concerning wall-temperature-ratio and unit-Reynolds-number effects, remained unchanged.

Having addressed this sensitivity question, some final comments are offered concerning transition-zone-asymmetry on sharp, slender cones at angle of attack. If one reviews the individual data sets 29,30,31 averaged by Potter^{16,17} to establish the family of curves shown in Figure 16, significant variations, similar to those witnessed in Figure 24, become evident (Figure 18 of Reference 16 shows a detailed comparison of these three data sets). In particular, the hypersonic ($M_\infty = 10$) data of DiCristina³⁰ show a local maximum in ($X_{TR}/X_{TR}, \alpha = 0^\circ$) near $\phi \approx 90^\circ$, while the lower Mach number data ($M_\infty < 8$) of Martellucci⁴⁴ and Mateer³¹ show a monotonic decay in this parameter as ϕ increases from 0° to 180° . The point is that, while it is generally accepted that transition moves rearward on the windward ray, and forward on the leeward ray, as angle of attack is increased, a complete understanding or description of the shape of the transition front between these extremes does not appear to be in hand.

VI. CONCLUSIONS

Boundary-layer transition experiments were conducted on sharp, slender cones in an aeroballistics range as part of the coordinated program for transition research recommended by the U.S. Transition Study Group. These tests were conducted at a nominal freestream Mach number of 4.5, on polished, five-degree half-angle cones; data acquisition was accomplished with dual-plane spark shadowgraphs. The primary independent variable was the wall-to-adiabatic wall temperature ratio, $(T_w/T_{aw})_e$, which was varied from $\approx .5$ to $\approx .2$ at each of two distinct edge unit Reynolds numbers, $(U_e/\nu_e) = 0.94$ and $2.82 \times 10^6/\text{inch}$. In addition, unit-Reynolds-number influence on transition was investigated, at $(T_w/T_{aw})_e \approx .22$, over the regime $0.48 < (U_e/\nu_e) < 2.84 \times 10^6/\text{inch}$. Transition-zone-asymmetry data, as a function of cone angle of attack, were also generated. The following observations were made:

1. Transition reversals with increased wall cooling were observed at both unit Reynolds numbers tested. At $2.82 \times 10^6/\text{inch}$, cooling was noted to be destabilizing in the regime $\approx .5 > (T_w/T_{aw})_e > \approx .35$, and stabilizing for $\approx .35 > (T_w/T_{aw})_e > \approx .23$. At $0.94 \times 10^6/\text{inch}$, cooling in the regime $\approx .45 > (T_w/T_{aw})_e > \approx .3$ yielded no discernable trends, whereas a definite stabilizing influence was evident for $\approx .3 > (T_w/T_{aw})_e > \approx .22$.
2. Data obtained at $(U_e/\nu_e) > \approx 10^6/\text{inch}$ showed a strong unit-Reynolds-number influence on transition, consistent with results observed by Potter, while data obtained at $(U_e/\nu_e) < \approx 10^6/\text{inch}$ indicated a lessening influence of unit Reynolds number on transition.
3. Pairing of transition Reynolds numbers measured at 0.94 and $2.82 \times 10^6/\text{inch}$, for each nominal wall temperature ratio tested, showed a unit-Reynolds-number influence on transition to exist over the entire $(T_w/T_{aw})_e$ regime tested.
4. Observed trends of transition Reynolds number with $(T_w/T_{aw})_e$ and (U_e/ν_e) , as measured on the cone's most-windward ray, were found, via a sensitivity study, to be unaffected by the angle-of-attack correction procedure utilized.

5. Transition-zone-asymmetry data in the regime $0 < (\alpha/\theta_c) < .63$, as measured on the cone's three most-leeward rays, were found to be consistent with an empirical model reported by Potter. As angle of attack increased, leeward-ray transition locations were noted to move increasingly forward. However, comparisons of present data and Potter's curves with other Mach five data illustrated that transition-zone-asymmetry may not be adequately described by a singular dependence on (α/θ_c) .

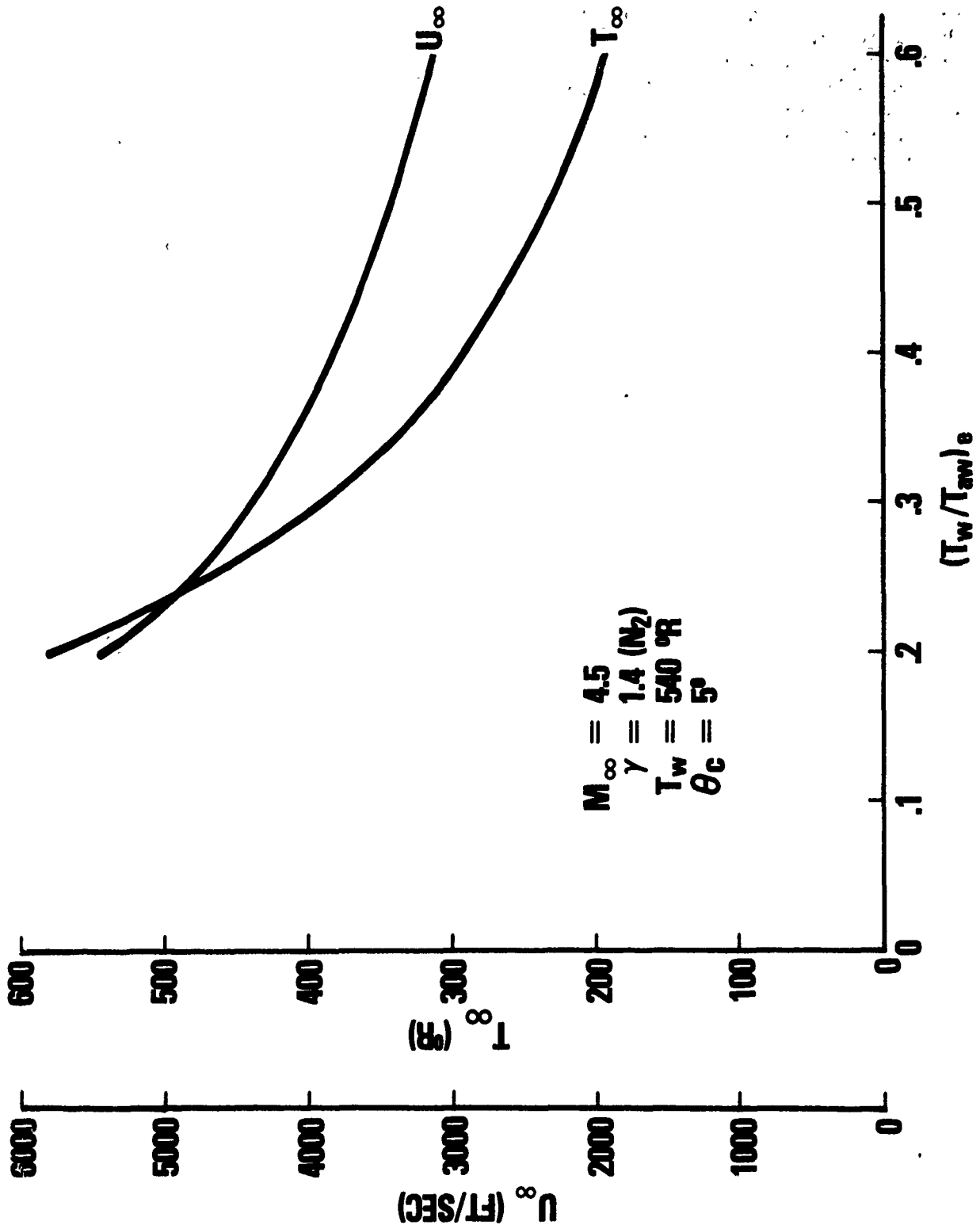


FIGURE 1 DEFINITION OF TEST CONDITIONS; VELOCITY AND TEMPERATURE

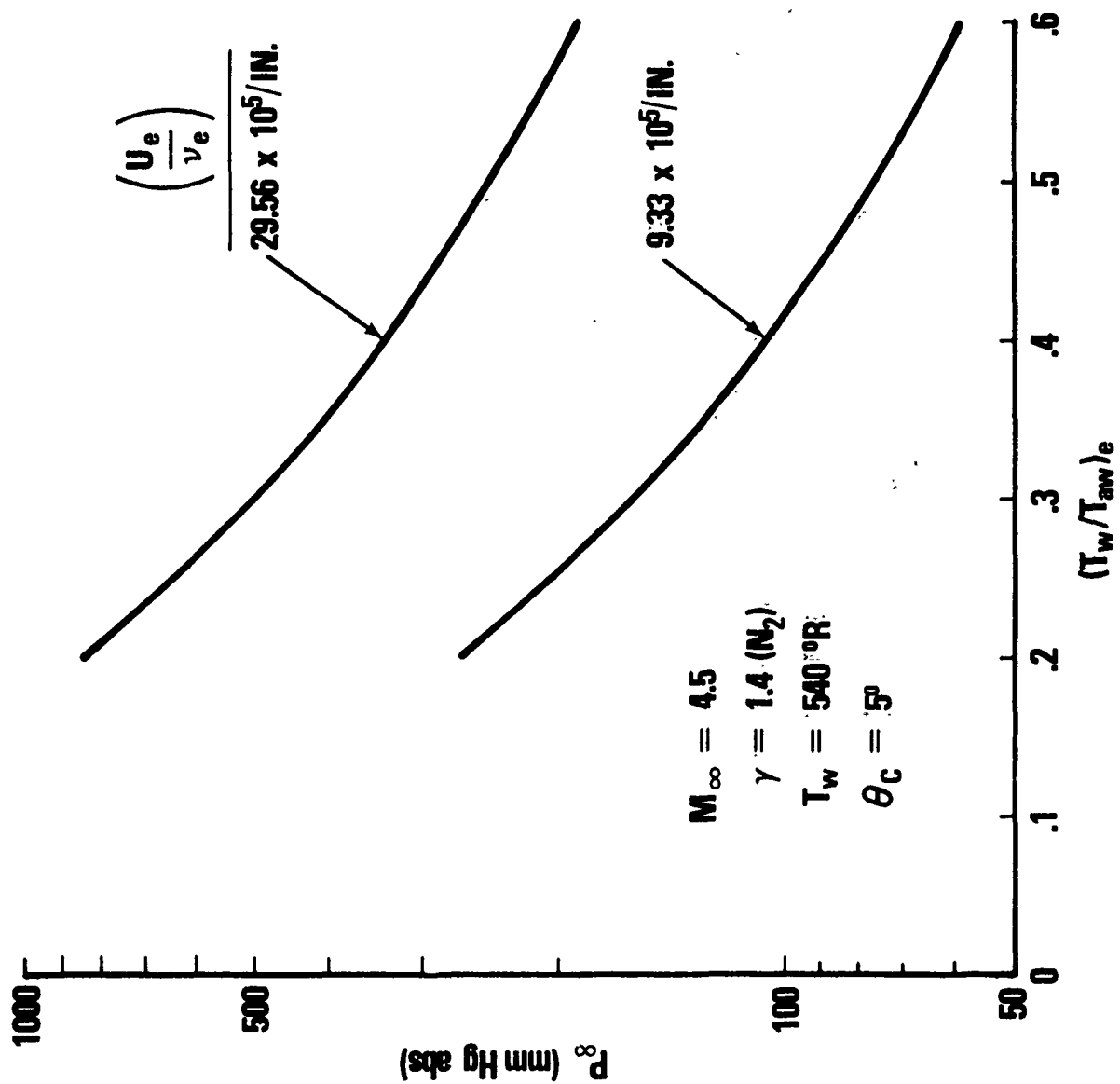


FIGURE 2 DEFINITION OF TEST CONDITIONS; PRESSURE

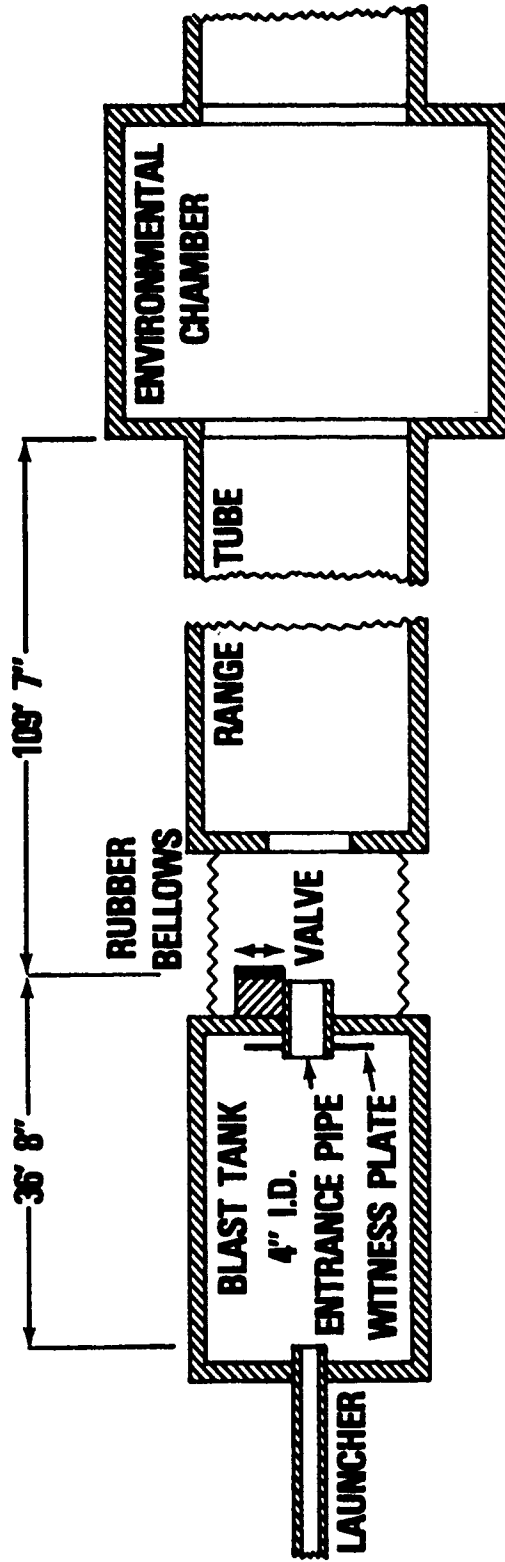


FIGURE 3 RANGE SCHEMATIC

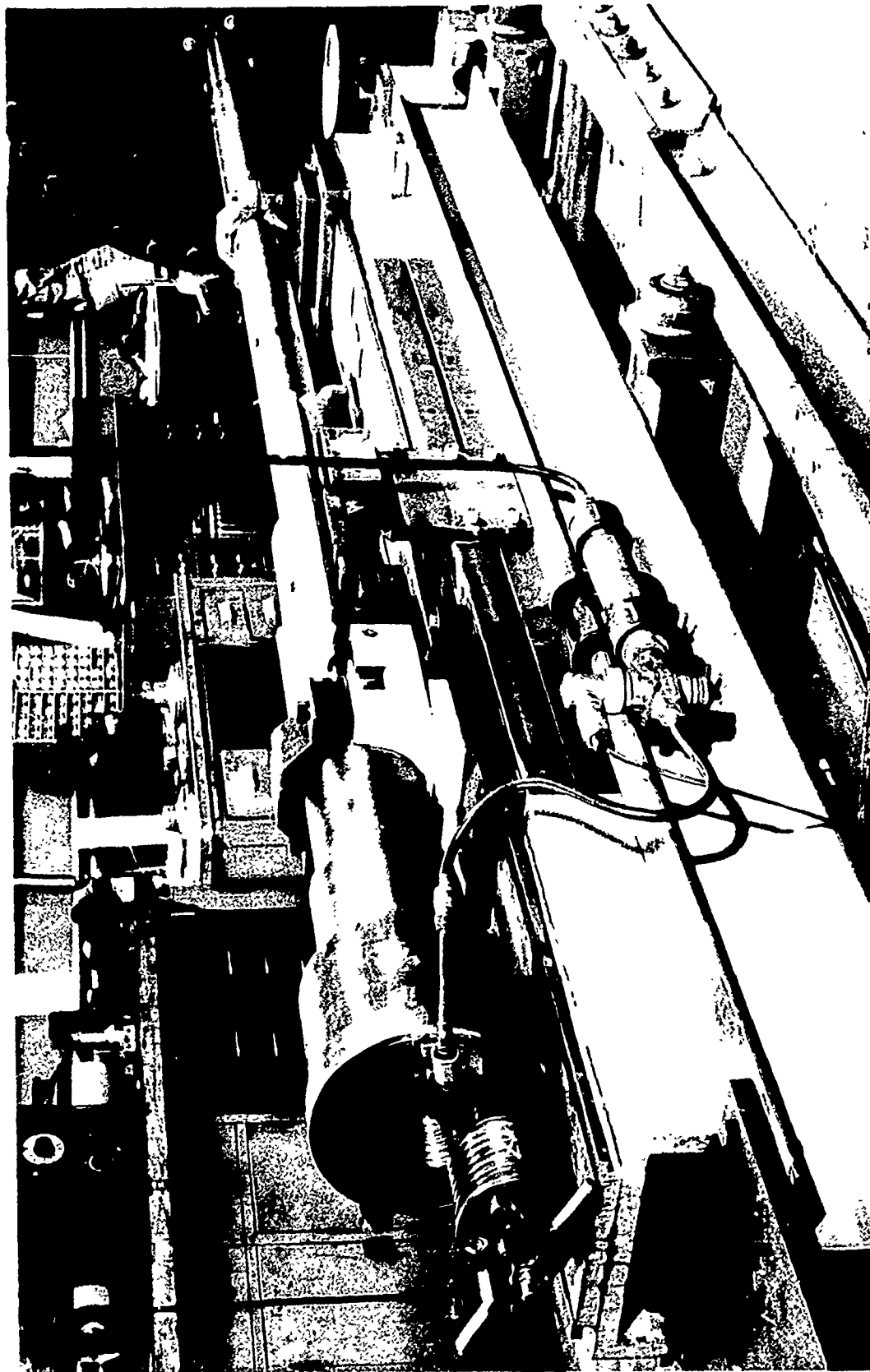


FIGURE 4 PHOTOGRAPH OF LAUNCHER

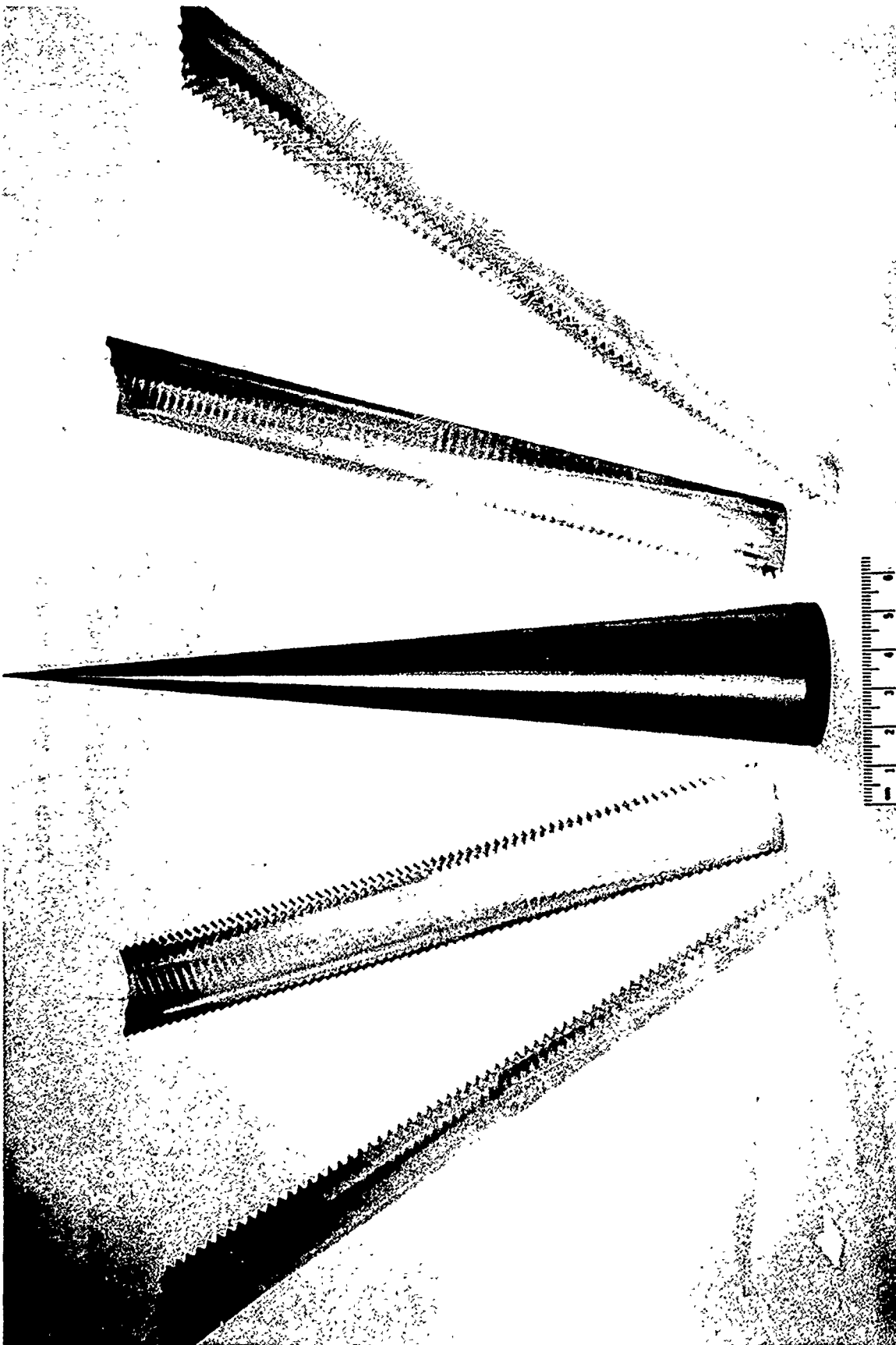


FIGURE 5 PHOTOGRAPH OF MODEL AND SABOT

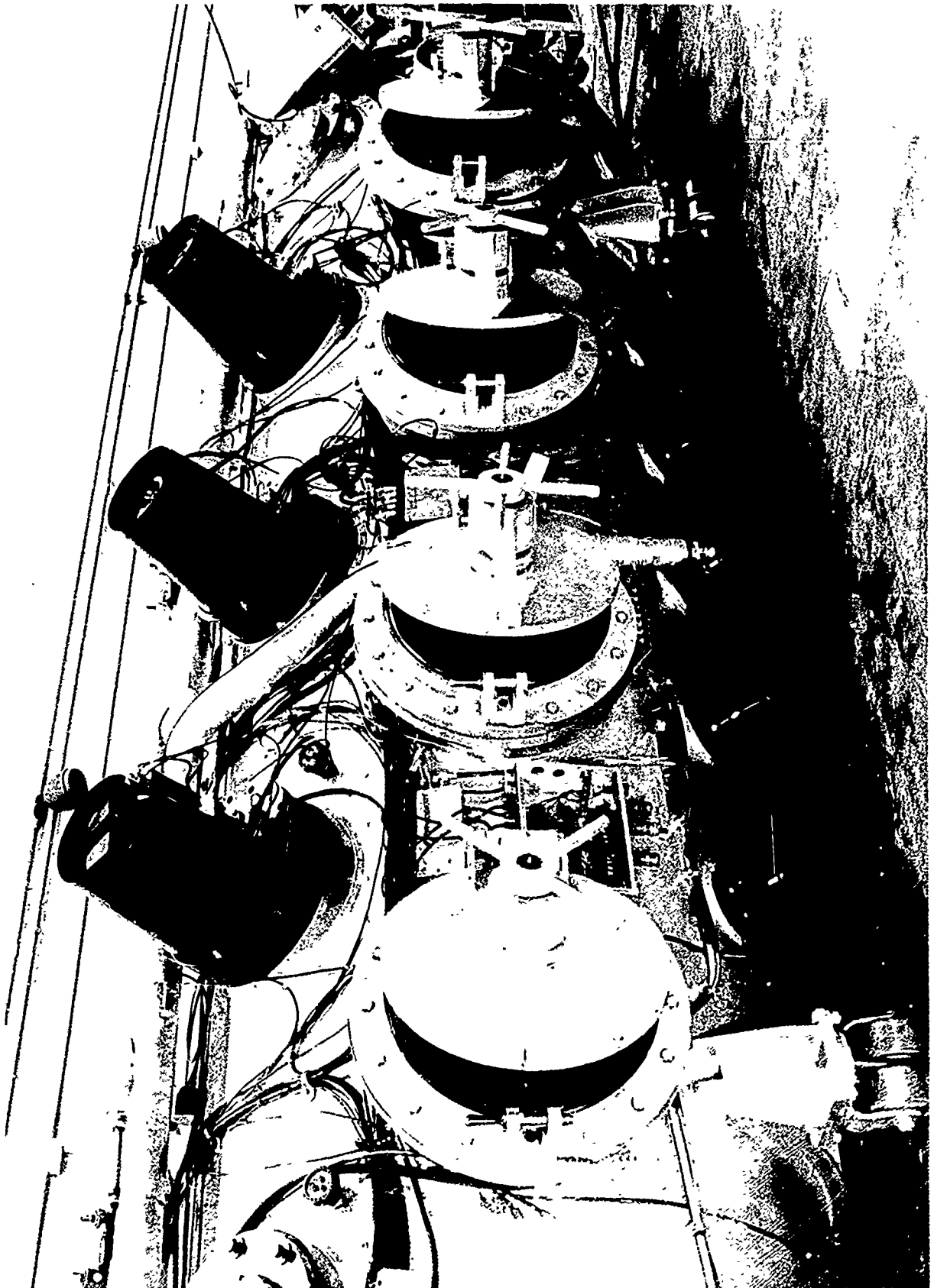


FIGURE 6 PHOTOGRAPH OF ENVIRONMENTAL CHAMBER

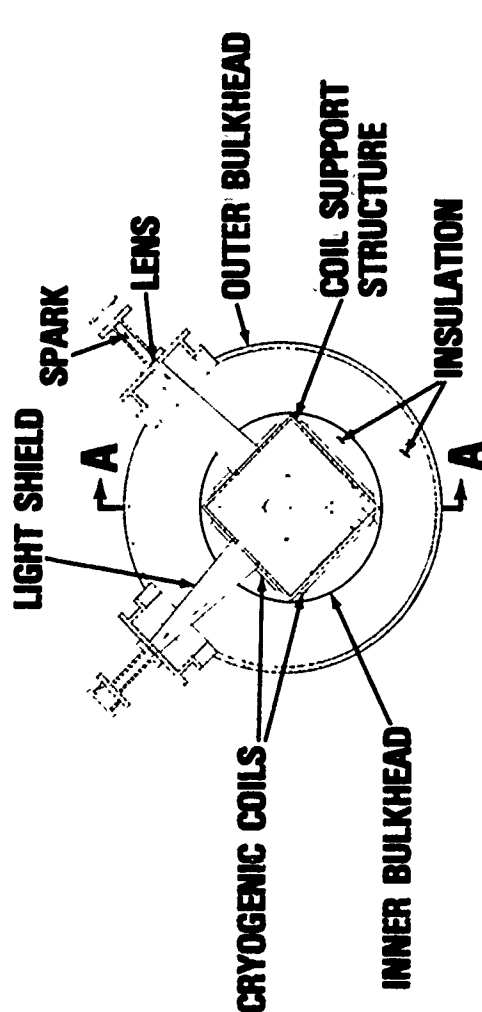
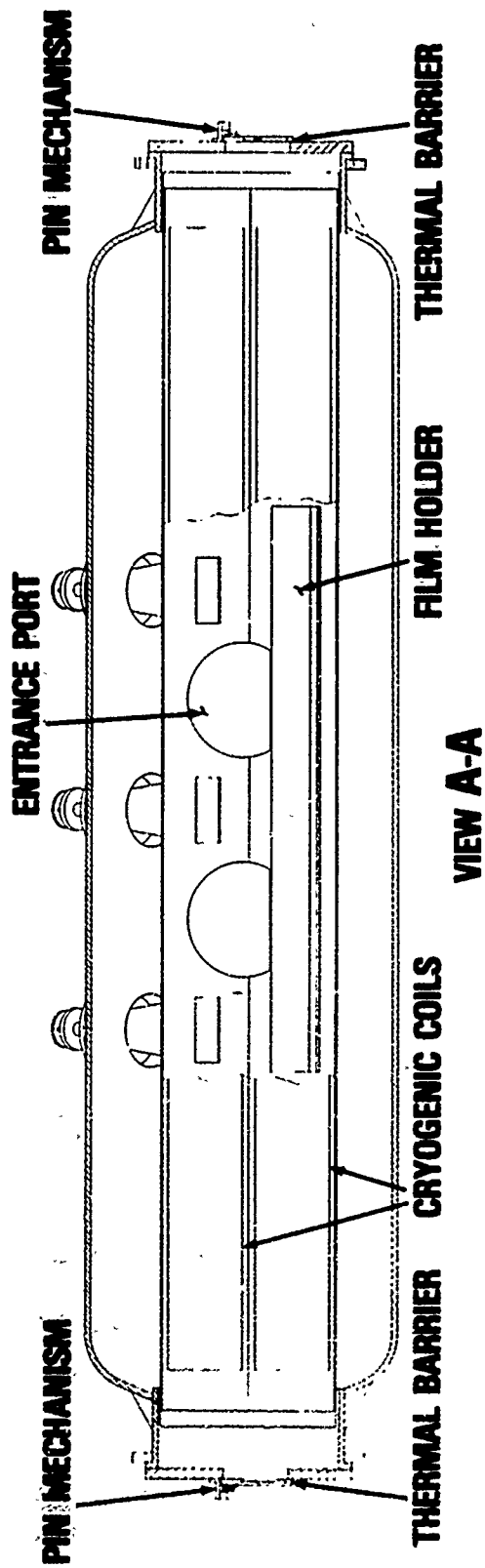


FIGURE 7 INTERNAL SCHEMATIC OF ENVIRONMENTAL CHAMBER

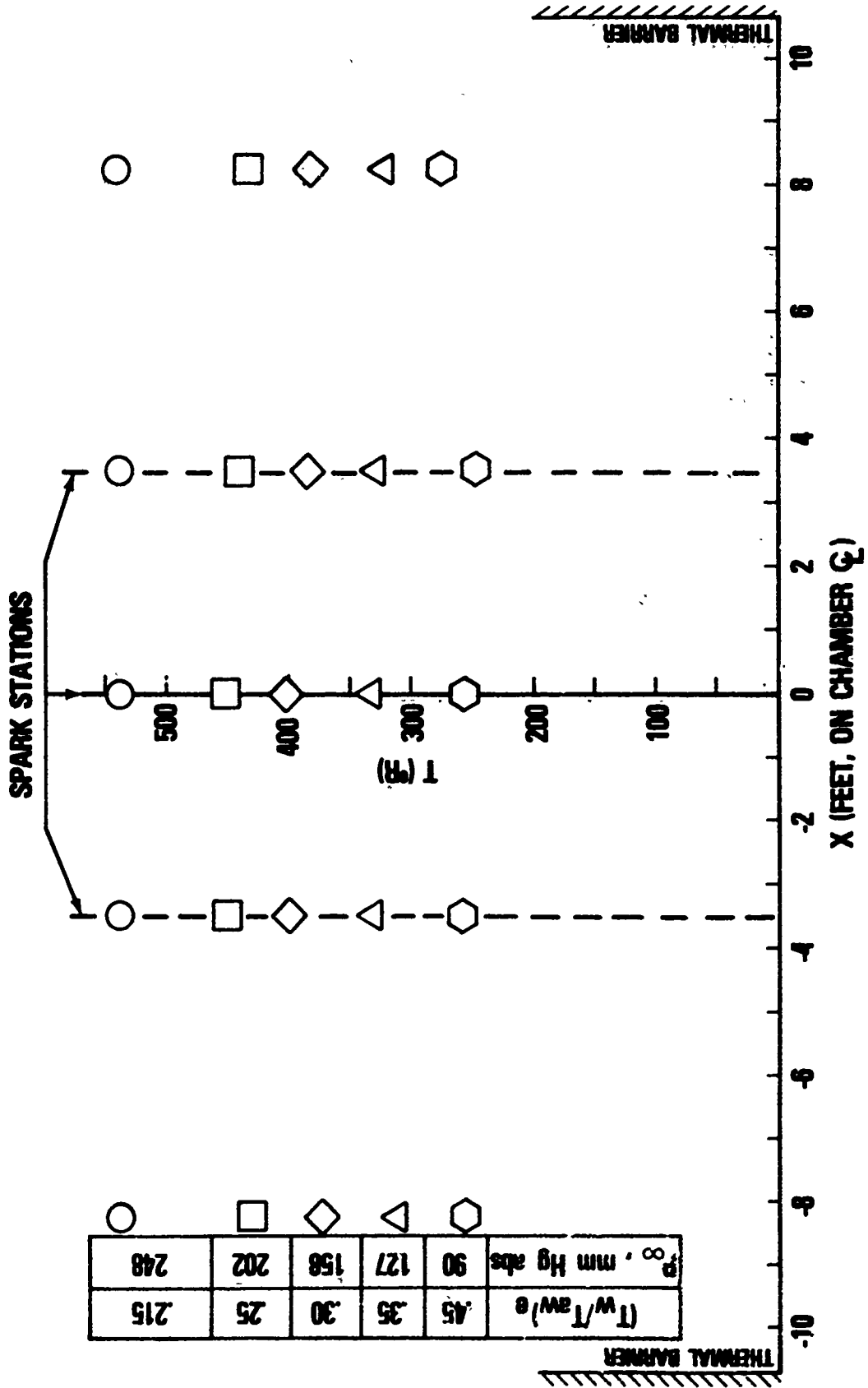


FIGURE 8 THERMAL CALIBRATION OF CHAMBER; HORIZONTAL TEMPERATURE DISTRIBUTIONS

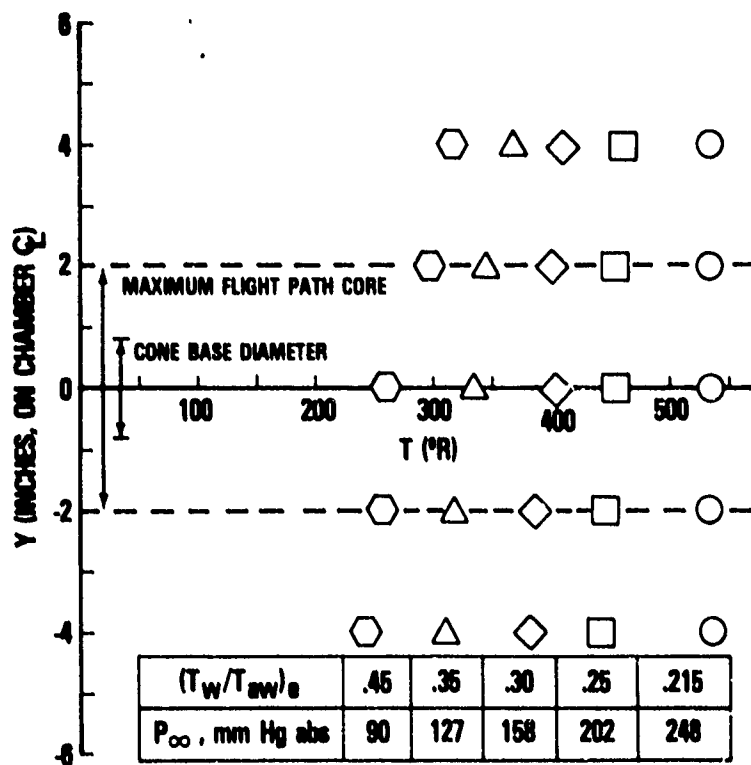


FIGURE 9 THERMAL CALIBRATION OF CHAMBER; VERTICAL TEMPERATURE DISTRIBUTIONS

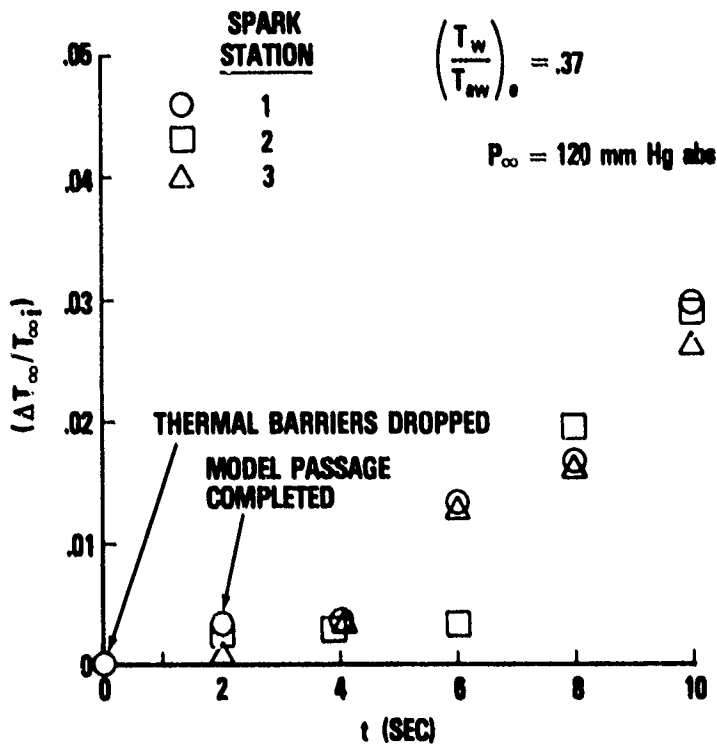
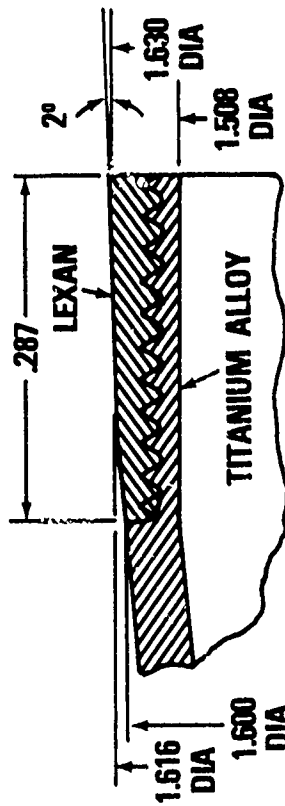
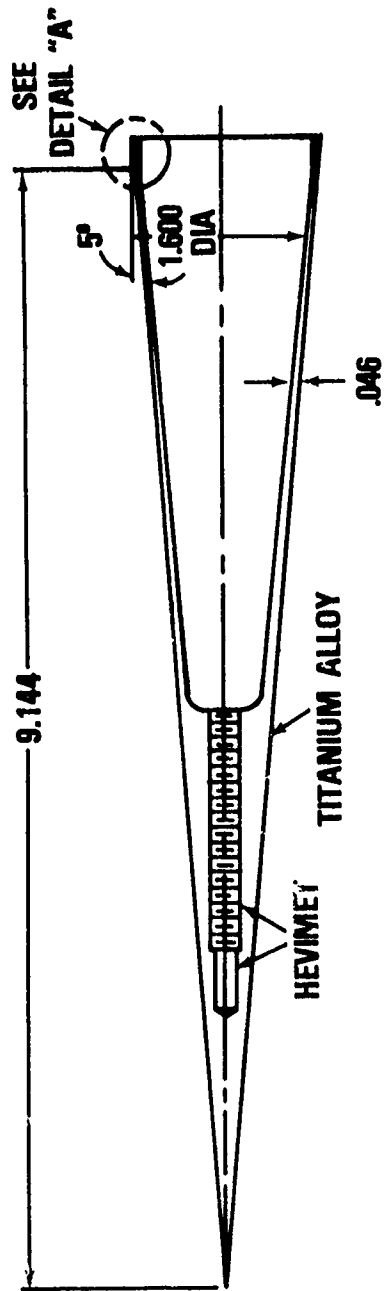


FIGURE 10 THERMAL CALIBRATION OF CHAMBER; TRANSIENT RESPONSE



DETAIL "A"

CPN = 67.2% MODEL WT. = 169 GRAMS

CGN = 55.9% PKG. WT. = 350 GRAMS

S.M. = 11.3%

FIGURE 11 MODEL SCHEMATIC

SYM.	P_{∞} (mm Hg, abs)	U_e/ν_e , 1/IN.
◇	499	1.95×10^6
□	630	2.50×10^6
○	762	2.84×10^6

OPEN: GLASS PLATES, RANGE-TUBE STATIONS

FILLED: TRI-X FILM, CHAMBER STATIONS

$T_{\infty} \cong 530$ °R, $(T_w/T_{aw})_e \cong .22$ FOR ALL

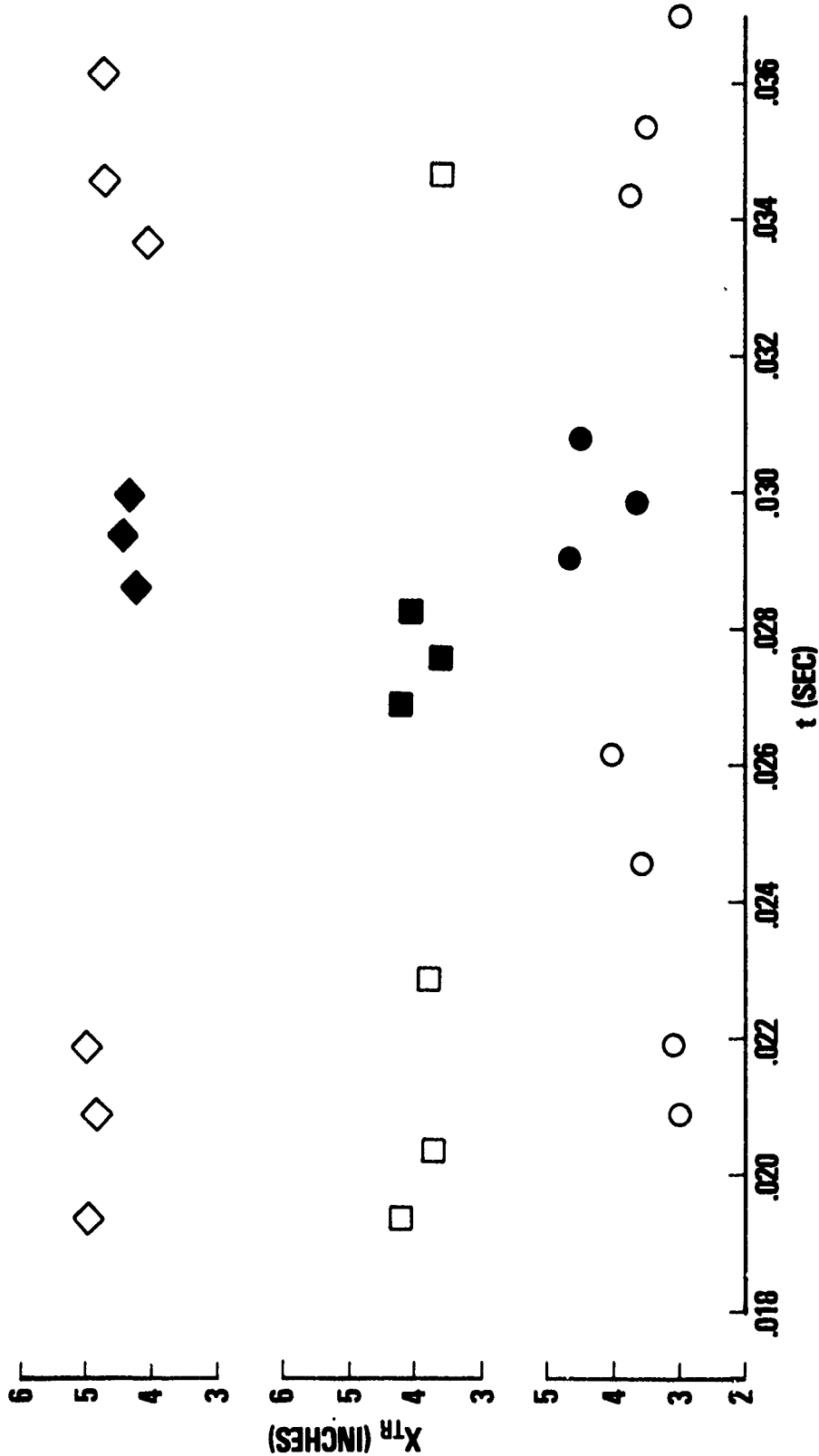


FIGURE 12 TRANSITION RUN LENGTH VS. TIME OF FLIGHT FOR THREE MOST SEVERE HEATING TRAJECTORIES

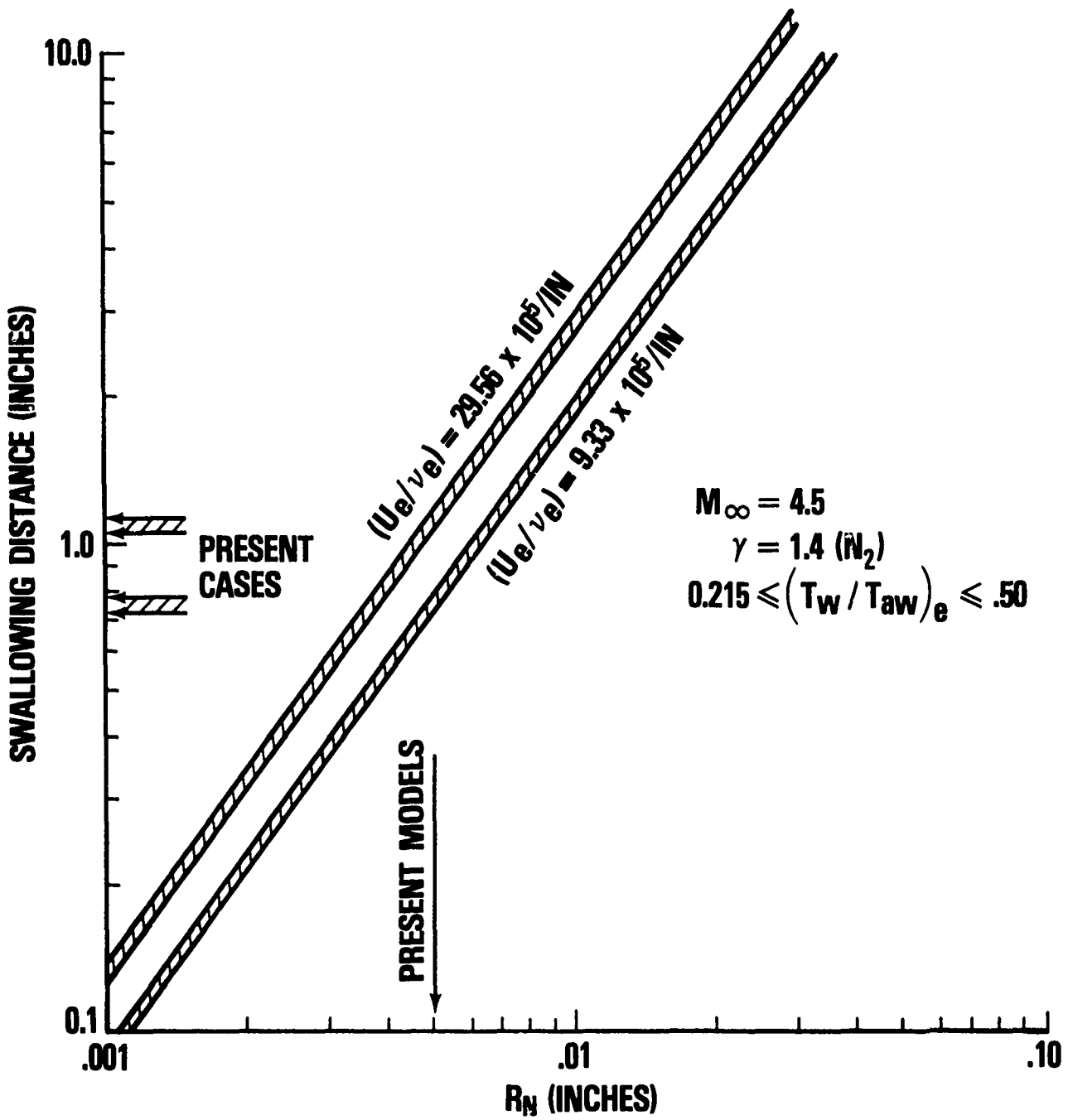


FIGURE 13 BLUNTNESS EFFECTS

NSWC/WOL TR 77-59

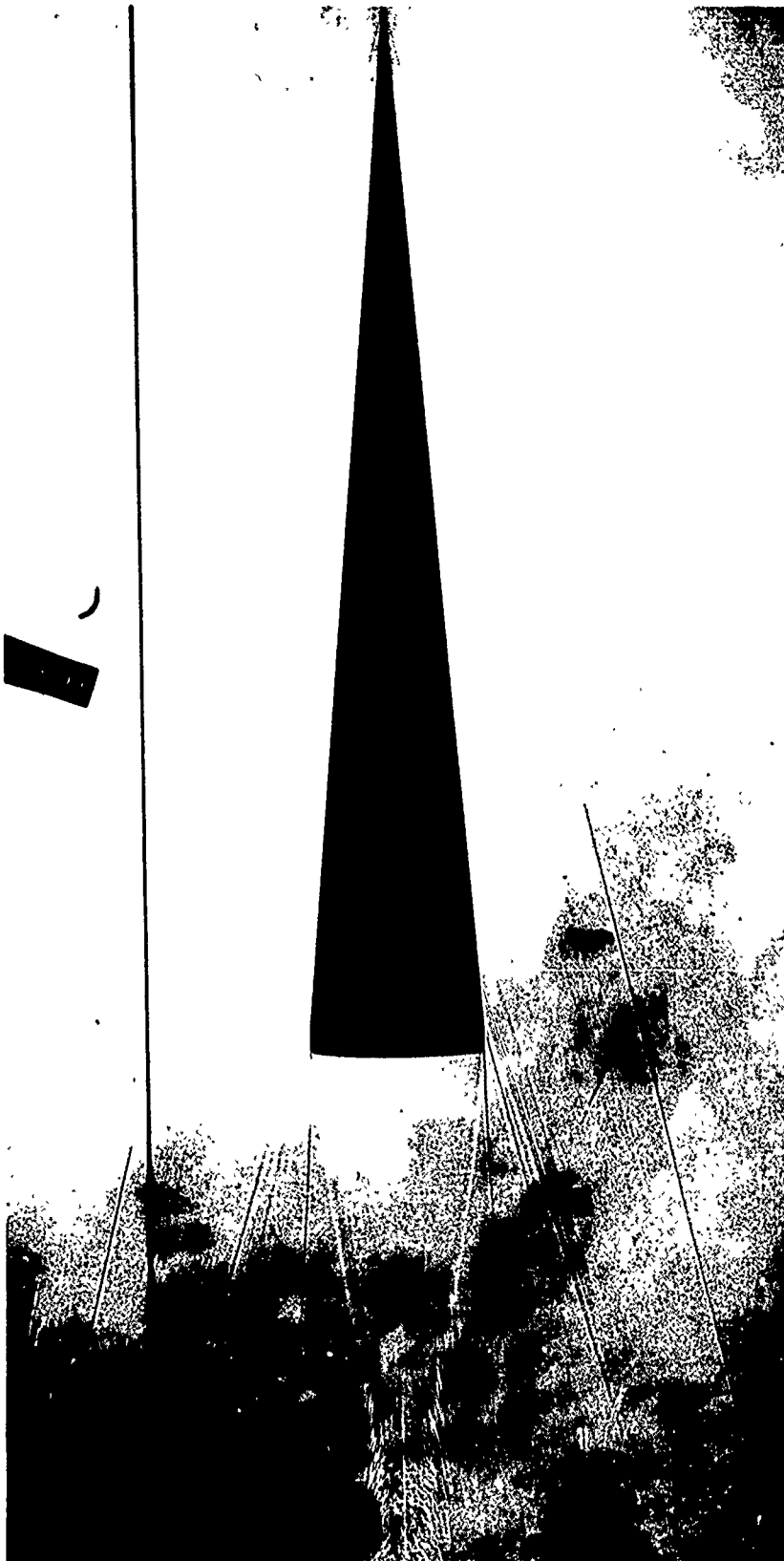


FIGURE 14 SPARK SHADOWGRAPH; ALL LAMINAR FLOW

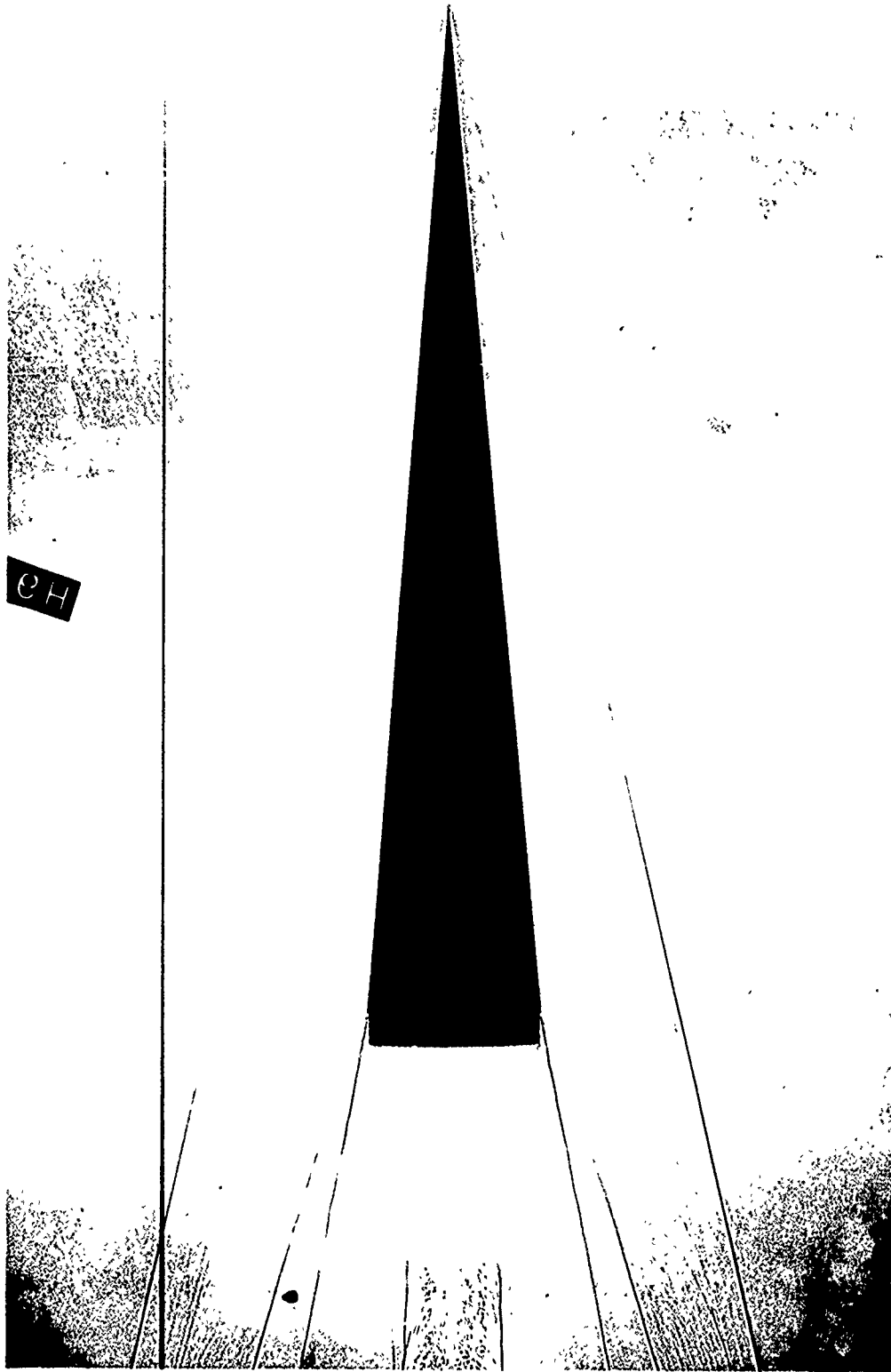


FIGURE 15 SPARK SHADOWGRAPH; TRANSITIONAL FLOW

**PRIMARY-RAY DATA ($\phi < 45^\circ$) OF PRESENT STUDY
CORRECTED FOR $\phi > 0^\circ$, $\alpha > 0^\circ$ BASED ON POTTER'S
 $\phi = 0^\circ$ & 60° CURVES.**

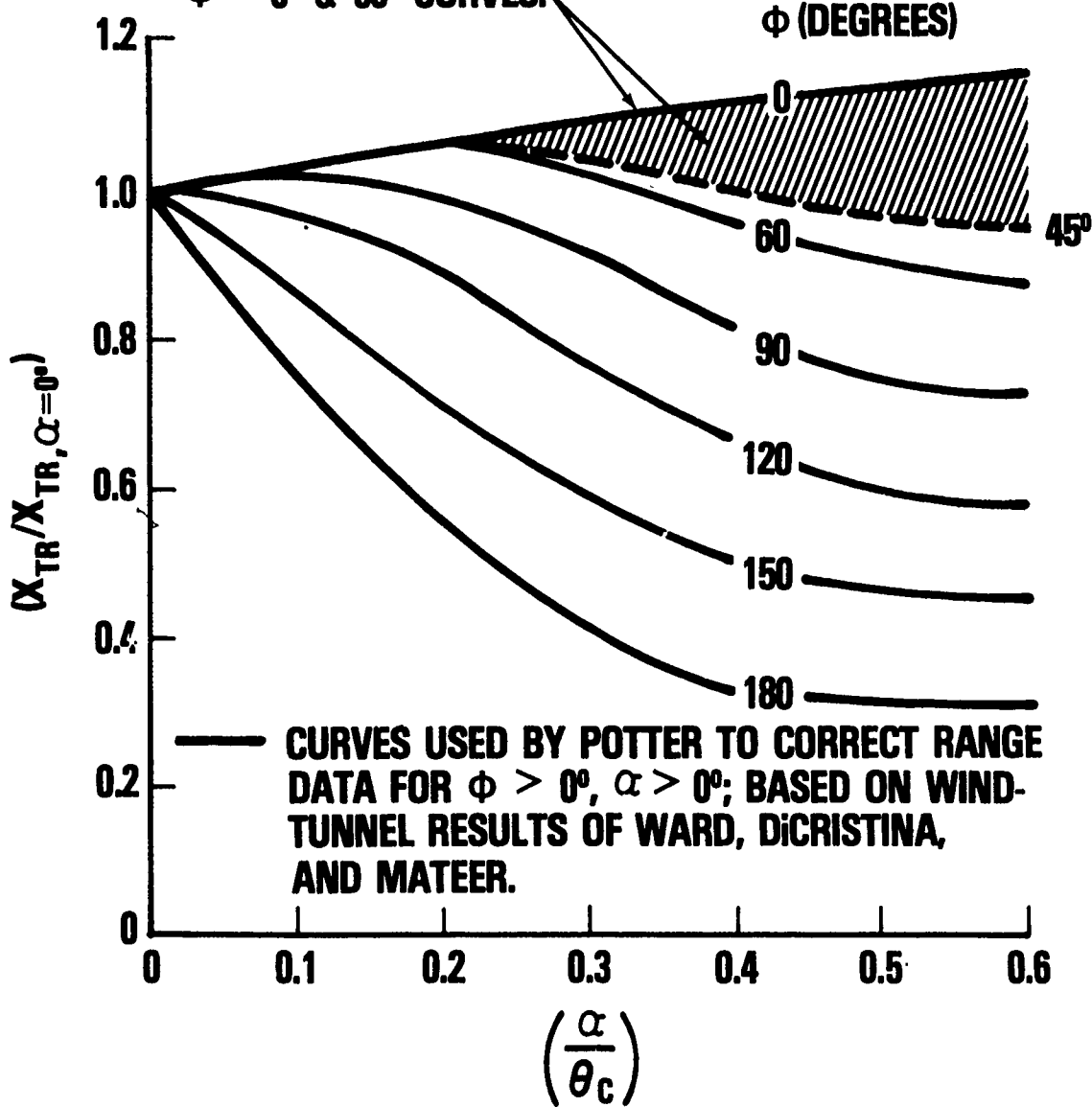


FIGURE 16 TRANSITION ZONE ASYMMETRY DUE TO ANGLE OF ATTACK, AS REPORTED BY POTTER

NSWC/WOL TR 77-59

TABLE 1
SUMMARY OF PRIMARY-RAY DATA

SHOT #	U_{∞}	T_{∞}	M_{∞}	P_{∞}	M_e	U_e/ν_e	U_e^2/ν_e	$\left(\frac{T_w}{T_{aw}}\right)_e$	(α/β_c)	ϕ	$\left(\frac{X_{TR}}{X_{TR} \alpha=0^\circ}\right)$	X_{TR}	X_{TR}	Re_{TR}
-	(FT/SEC)	(R)	-	(MM Hg, abs)	-	(1/INCH)	(1/SEC)	-	-	(DEG)	-	(IN, READ)	(IN, CORR.)	-
6723	4910	526	4.29	762	4.08	2.84×10^6	1.66×10^{11}	0.237	0.017	32.2	1.007	4.71	4.68	1.33×10^7
↓									0.018	12.0	1.007	3.68	3.66	1.04×10^7
6731	4756	464	4.43	640	4.21	2.92×10^6	1.65×10^{11}	0.257	0.031	41.2	1.013	4.56	4.50	1.28×10^7
↓									0.035	2.3	1.014	4.02	3.96	1.16×10^7
6726	4305	390	4.37	500	4.15	2.81×10^6	1.44×10^{11}	0.311	0.050	6.6	1.020	3.13	3.07	8.96×10^6
↓									0.047	27.1	1.019	3.61	3.54	1.04×10^7
6729	4201	329	4.64	404	4.40	3.08×10^6	1.54×10^{11}	0.336	0.120	36.9	1.038	2.86	2.75	7.74×10^6
↓									0.097	33.9	1.029	2.90	2.81	7.91×10^6
6727	3785	295	4.42	334	4.20	2.78×10^6	1.25×10^{11}	0.405	0.063	3.9	1.023	2.60	2.54	7.82×10^6
↓									0.043	5.7	1.017	2.69	2.64	8.13×10^6
6730	3441	265	4.24	291	4.03	2.66×10^6	1.09×10^{11}	0.480	0.046	39.2	1.019	2.53	2.48	7.65×10^6
↓									0.080	37.2	1.026	2.93	2.85	7.91×10^6
6728	3352	243	4.31	248	4.10	2.62×10^6	1.04×10^{11}	0.510	0.088	17.1	1.028	3.04	2.96	8.21×10^6
↓									0.078	16.8	1.026	2.78	2.71	7.53×10^6
6715	5054	535	4.38	230	4.16	8.64×10^5	5.18×10^{10}	0.226	0.315	21.2	1.073	3.47	3.24	8.62×10^6
↓									0.401	19.0	1.071	2.63	2.46	6.54×10^6
6732	4796	465	4.46	202	4.23	9.26×10^5	5.27×10^{10}	0.253	0.415	14.0	1.084	2.67	2.47	6.57×10^6
↓									0.322	25.0	1.067	3.52	3.30	8.66×10^6
6719	4388	370	4.57	156	4.34	9.97×10^5	5.20×10^{10}	0.306	0.303	23.9	1.070	4.75	4.44	1.16×10^7
↓									0.274	27.8	1.066	5.70	5.34	1.40×10^7
6734	4076	339	4.44	128	4.21	8.83×10^5	4.27×10^{10}	0.350	0.480	43.0	0.977	*8.07	*8.26	*7.13 x 10 ⁶
↓									0.480	43.0	0.981	*8.13	*8.26	*7.16 x 10 ⁶
6717	3850	276	4.65	108	4.40	1.05×10^6	4.79×10^{10}	0.400	0.255	24.7	1.058	19.13	-	18.45×10^6
↓									0.295	27.3	1.066	19.13	-	18.45×10^6
6720	3863	274	4.68	105	4.43	1.04×10^6	4.78×10^{10}	0.398	0.286	25.9	1.068	19.13	-	18.45×10^6
↓									0.286	25.9	1.068	19.13	-	18.45×10^6
6718	3627	242	4.68	76	4.43	8.95×10^5	3.85×10^{10}	0.451	0.028	13.2	1.011	4.30	4.25	4.24×10^6
↓									0.049	35.6	1.020	3.56	3.49	3.48×10^6
6724	4939	530	4.30	128	4.09	4.75×10^5	2.78×10^{10}	0.235	0.126	37.1	1.040	4.18	4.02	4.01×10^6
↓									0.126	37.1	1.040	4.18	4.02	4.01×10^6
6715	(SEE ABOVE)								0.144	0.3	1.047	5.87	5.61	4.95×10^6
6737	5183	530	4.51	370	4.28	1.46×10^6	8.98×10^{10}	0.218	0.198	5.4	1.064	5.89	5.53	4.89×10^6
↓									0.187	28.0	1.061	5.23	4.93	4.36×10^6
6725	5174	532	4.50	499	4.27	1.95×10^6	1.20×10^{11}	0.218	0.187	28.0	1.061	5.23	4.93	4.36×10^6
↓									0.376	25.1	1.059	5.07	4.79	5.02×10^6
6738	5172	528	4.51	630	4.28	2.50×10^6	1.53×10^{11}	0.219	0.526	27.1	1.041	3.82	3.70	3.82×10^6
↓									0.381	32.7	1.041	4.04	3.88	4.05×10^6
6723	(SEE ABOVE)								0.594	17.0	1.066	5.45	5.01	4.49×10^6
↓									0.526	15.8	1.087	5.12	4.70	4.21×10^6
									0.267	12.8	1.077	19.13	-	14.34×10^6
									0.223	12.8	1.069	19.13	-	14.34×10^6
									0.171	0.2	1.056	19.13	-	14.34×10^6
									0.451	5.5	1.112	5.78	5.20	7.59×10^6
									0.506	14.8	1.091	5.39	4.94	7.21×10^6
									0.524	20.6	1.067	5.24	4.91	7.18×10^6
									0.062	43.4	1.022	4.32	4.22	8.24×10^6
									0.045	25.8	1.018	4.52	4.44	8.67×10^6
									0.084	41.6	1.027	4.42	4.31	8.41×10^6
									0.196	17.9	1.064	4.50	4.23	1.06×10^7
									0.161	2.0	1.053	3.79	3.60	8.99×10^6
									0.172	19.7	1.057	4.27	4.04	1.01×10^7

*BURSTS OBSERVED. X_{TR} NOT DEFINED
†ALL LAMINAR

TABLE 2
AVERAGE VALUES AND MAXIMUM VARIABILITY OF TEST PARAMETERS

PARAMETER	WALL-TEMPERATURE RATIO DATA, HIGH (U_e/ν_e)	WALL-TEMPERATURE RATIO DATA, LOW (U_e/ν_e)	UNIT REYNOLDS NUMBER DATA
Me	4.17 +23 (+5.5%) -14 (-3.4%)	4.30 +13 (+3.0%) -14 (-3.3%)	4.20 +08 (+1.9%) -12 (-2.9%)
$\left(\frac{T_w}{T_{aw}}\right)_e$	—	—	0.225 +012 (+5.3%) -007 (-3.1%)
$\left(\frac{U_e}{\nu_e}\right)^*$	2.82×10^6 +26 (+9.2%) -20 (-7.1%)	9.42×10^5 +1.08 (+11.5%) -78 (-8.3%)	—
$\left(\frac{U_e^2}{\nu_e}\right)^{**}$	1.38×10^{11} +28 (+20.3%) -34 (-24.6%)	4.79×10^{10} +48 (+10.0%) -94 (-19.6%)	—

* PER INCH

** PER SECOND; NO ATTEMPT MADE TO HOLD CONSTANT

SYM.	θ_c	M_∞	M_e	$U_e/\nu_e, 1/IN.$	$U_e^2/\nu_e, 1/SEC.$	FACILITY
\triangle	5°	4.4	4.2	2.82×10^6	$1.04 - 1.66 \times 10^{11}$	RANGE
\circ		4.5	4.3	0.94×10^6	$0.39 - 0.53 \times 10^{11}$	

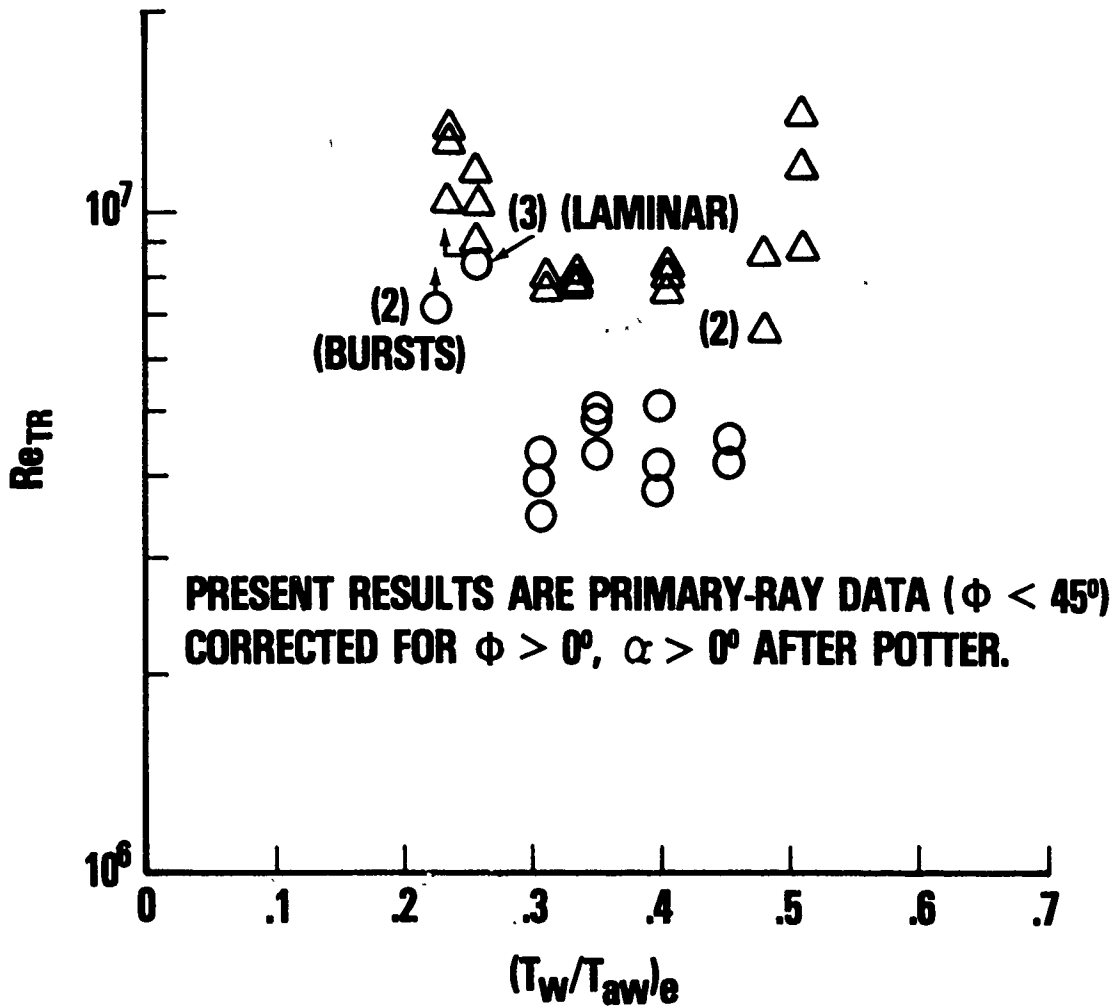


FIGURE 17 TRANSITION REYNOLDS NUMBER VS. WALL-TO-ADIABATIC WALL TEMPERATURE RATIO; PRESENT DATA

SOURCE	SYM.	θ_c	M_∞	M_e	$U_e/\nu_e, 1/IN.$	$U_e^2/\nu_e, 1/SEC.$	FACILITY
REDA	\triangle	5°	4.4	4.2	2.82×10^6	$1.04 - 1.66 \times 10^{11}$	RANGE
	\circ		4.5	4.3	0.94×10^6	$0.39 - 0.53 \times 10^{11}$	
POTTER	diagonal lines	10°	5.0	4.3	$\sim 3.0 \times 10^6$	$\sim 2.0 \times 10^{11}$	RANGE
	diagonal lines				$\sim 0.8 \times 10^6$	$\sim 0.53 \times 10^{11}$	
	horizontal lines	10°	2.3	2.1	$\sim 3.0 \times 10^6$	$\sim 0.90 \times 10^{11}$	
	\square				$\sim 0.9 \times 10^6$	$\sim 0.27 \times 10^{11}$	
SHEETZ	\diamond	5°	4.9	4.6	$\sim 2.2 \times 10^6$	$1.3 - 2.9 \times 10^{11}$	RANGE

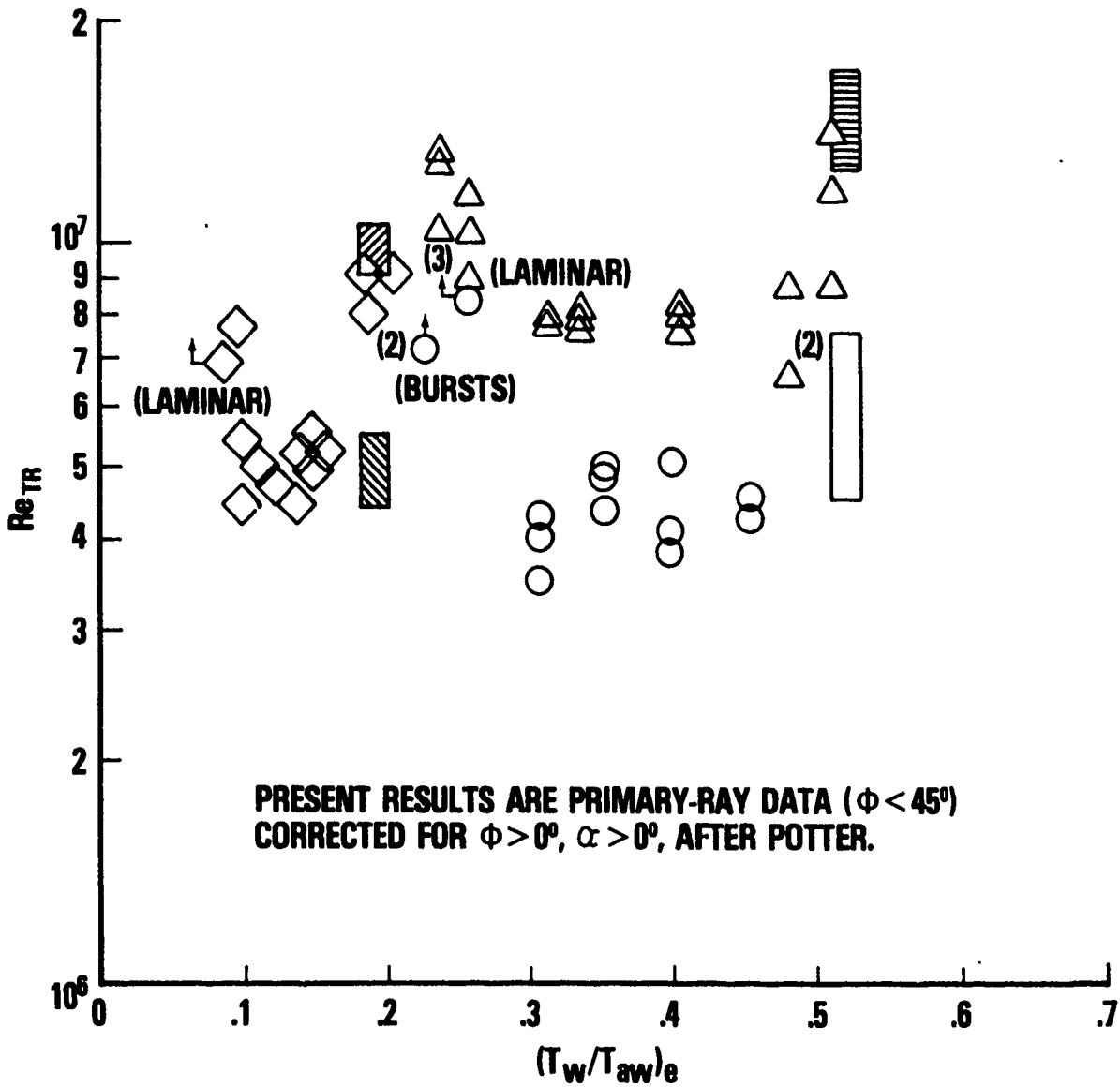


FIGURE 18 TRANSITION REYNOLDS NUMBER VS. WALL-TO-ADIABATIC WALL TEMPERATURE RATIO; PRESENT DATA VS. POTTER AND SHEETZ

SOURCE	SYM.	θ_c	M_∞	M_e	$U_e/\nu_e, 1/IN.$	$U_e^2/\nu_e, 1/SEC.$	FACILITY
REDA	\triangle	5°	4.4	4.2	2.82×10^6	$1.04 - 1.66 \times 10^{11}$	RANGE
	\circ		4.5	4.3	0.94×10^6	$0.39 - 0.53 \times 10^{11}$	
STETSON	\diamond	8°	5.5	4.9	$0.17 - 0.48 \times 10^6$	$0.09 - 0.29 \times 10^{11}$	SHOCK TUNNEL
KROGMANN	---	5°	5.0	4.7	0.46×10^6	$0.13 - 0.18 \times 10^{11}$	LUDWIG TUBE
	---				$0.33 - 0.79 \times 10^6$	$0.13 - 0.25 \times 10^{11}$	

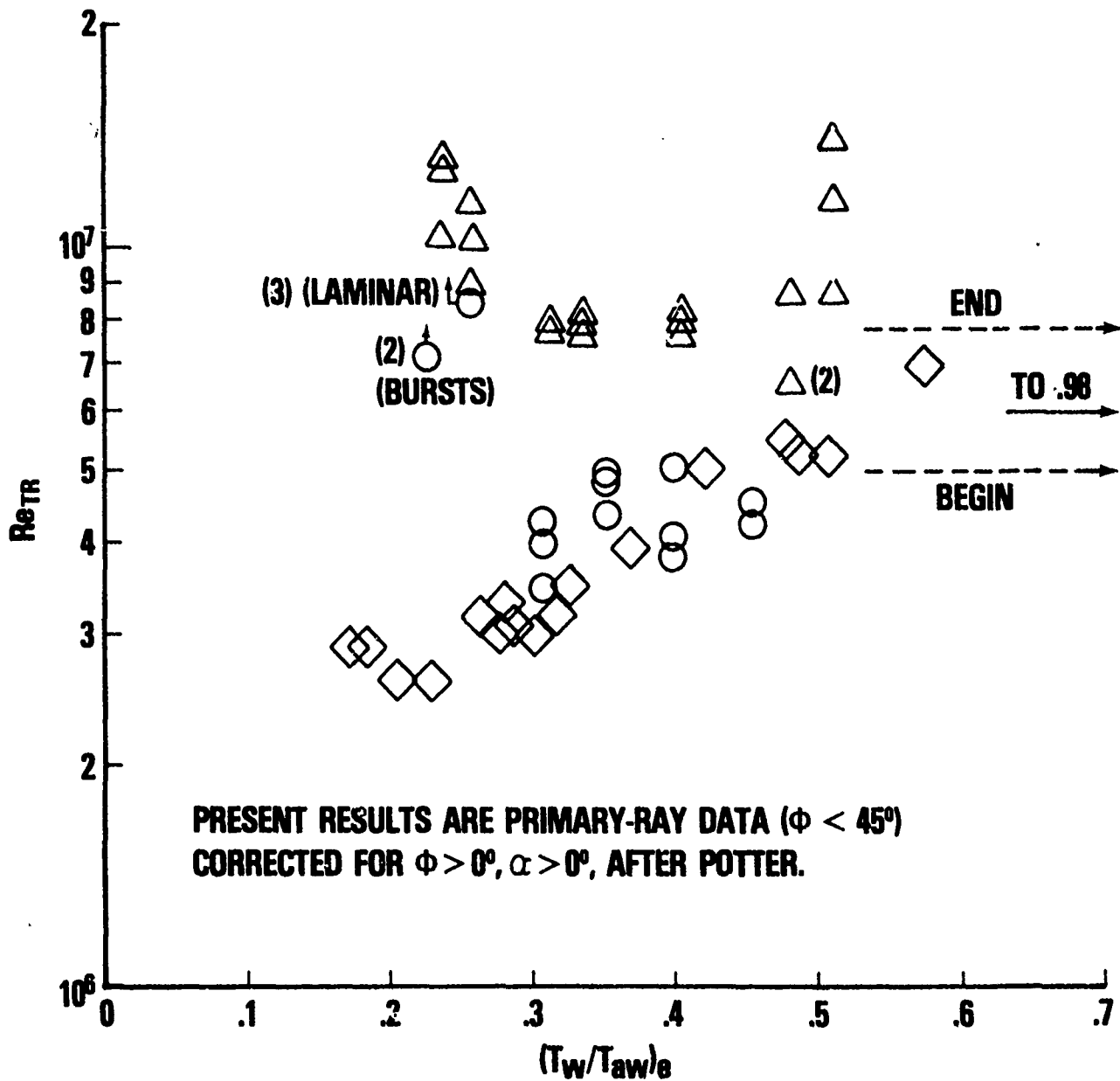


FIGURE 19 TRANSITION REYNOLDS NUMBER VS. WALL-TO-ADIABATIC WALL TEMPERATURE RATIO; PRESENT DATA VS. STETSON AND KROGMANN

SOURCE	SYM.	θ_c	M_∞	M_0	$(T_w/T_{aw})_0$	U_0^2/ν_0 , 1/SEC.	FACILITY
REDA	○	5°	4.4	4.2	.22	.28 - 1.66 x 10 ¹¹	RANGE
POTTER	---	10°	5.0	4.3	.19	.42 - 5.27 x 10 ¹¹	RANGE
		10°	2.3	2.1	.52	.17 - 1.00 x 10 ¹¹	RANGE
SHEETZ	□	5°	5.0	4.8	.19	1.40 - 1.71 x 10 ¹¹	RANGE

PRESENT RESULTS ARE PRIMARY-RAY DATA ($\phi < 45^\circ$)

CORRECTED FOR $\phi > 0^\circ$, $\alpha > 0^\circ$, AFTER POTTER

— LEAST-SQUARES FIT OF PRIMARY-RAY DATA, $(\frac{U_0}{\nu_0}) > 10^6/\text{IN.}$

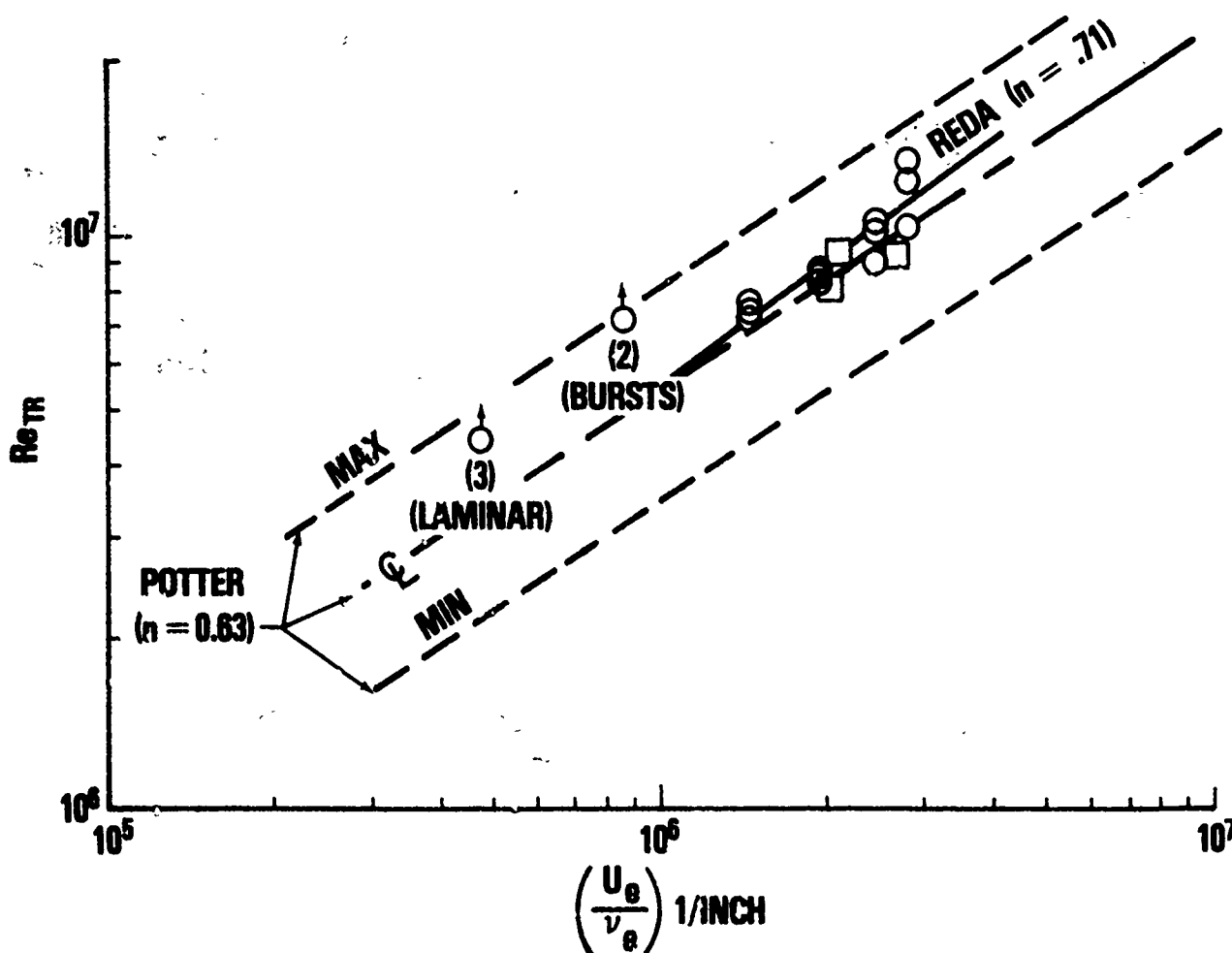


FIGURE 20 TRANSITION REYNOLDS NUMBER VS. UNIT REYNOLDS NUMBER; PRESENT DATA VS. POTTER AND SHEETZ

SOURCE	SYM.	θ_c	M_∞	M_e	$(T_w/T_{aw})_e$	U_e^2/ν_e , 1/SEC.	FACILITY
REDA	○	5°	4.4	4.2	.22	.28 - 1.66 x 10 ¹¹	RANGE
KROGMANN	---	5°	5.0	4.7	.79 - .67	.08 - 0.42 x 10 ¹¹	LUDWIG TUBE
STETSON	□	8°	5.5	4.9	.17 - .23	.11 - 0.29 x 10 ¹¹	SHOCK TUNNEL
	◇				.26 - .37	.09 - 0.26 x 10 ¹¹	
	△				.42 - .50	.14 - 0.17 x 10 ¹¹	
	○				.57	0.18 x 10 ¹¹	

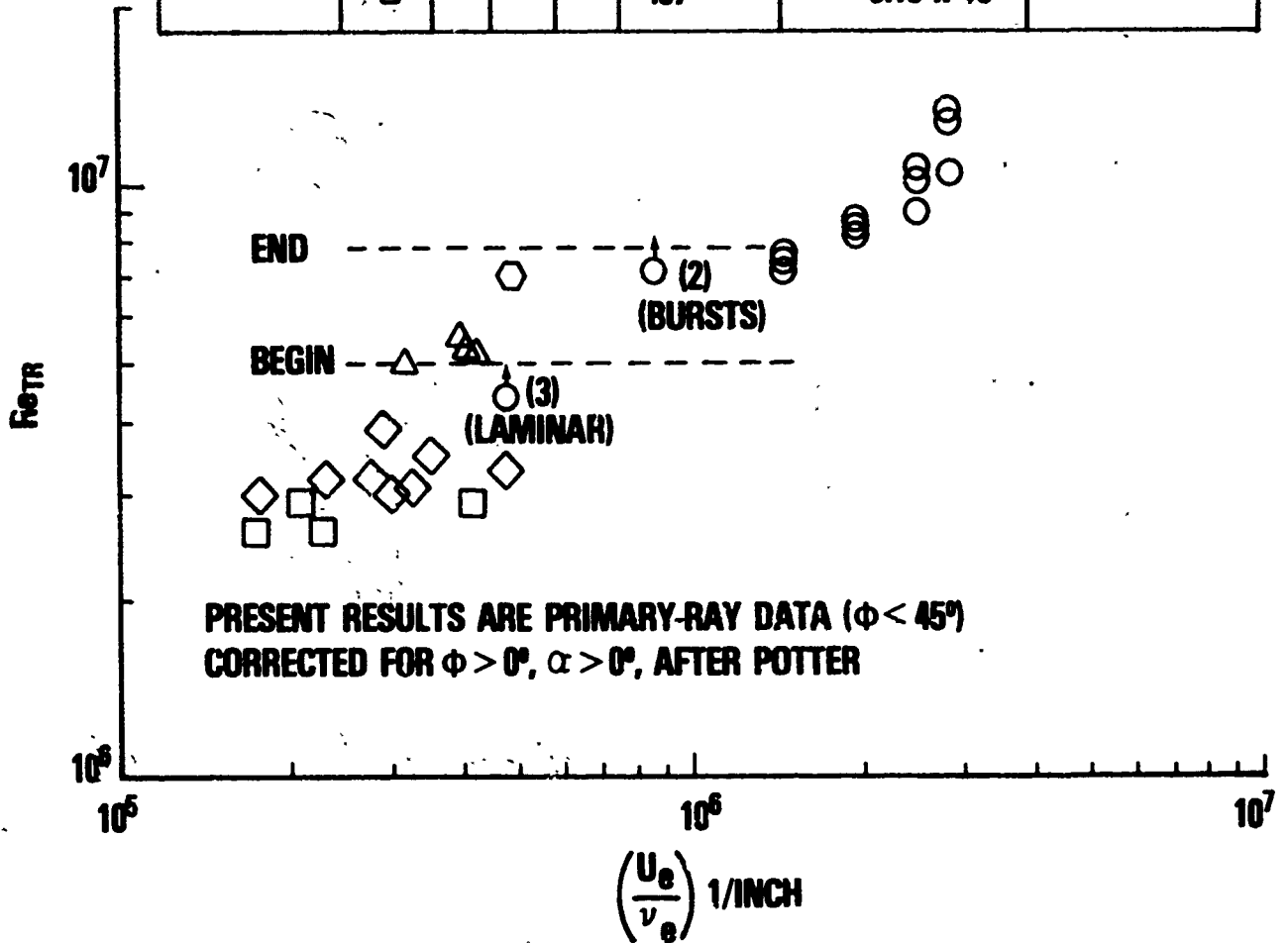


FIGURE 21 TRANSITION REYNOLDS NUMBER VS. UNIT REYNOLDS NUMBER; PRESENT DATA VS. KROGMANN AND STETSON

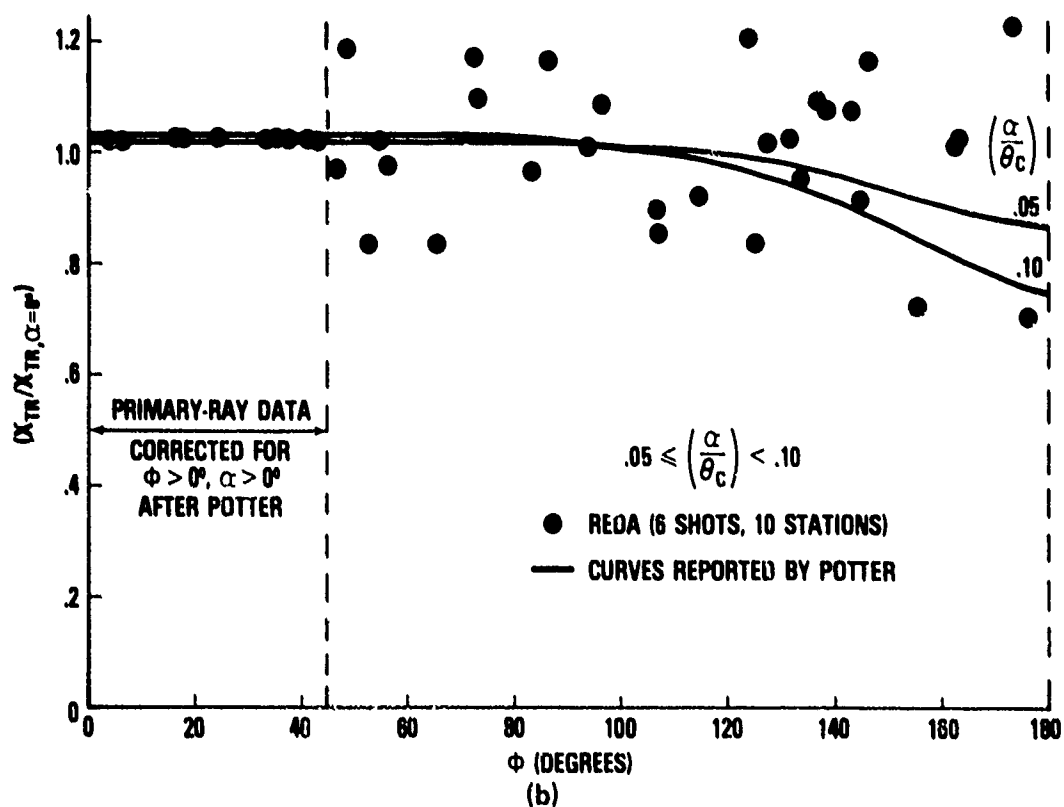
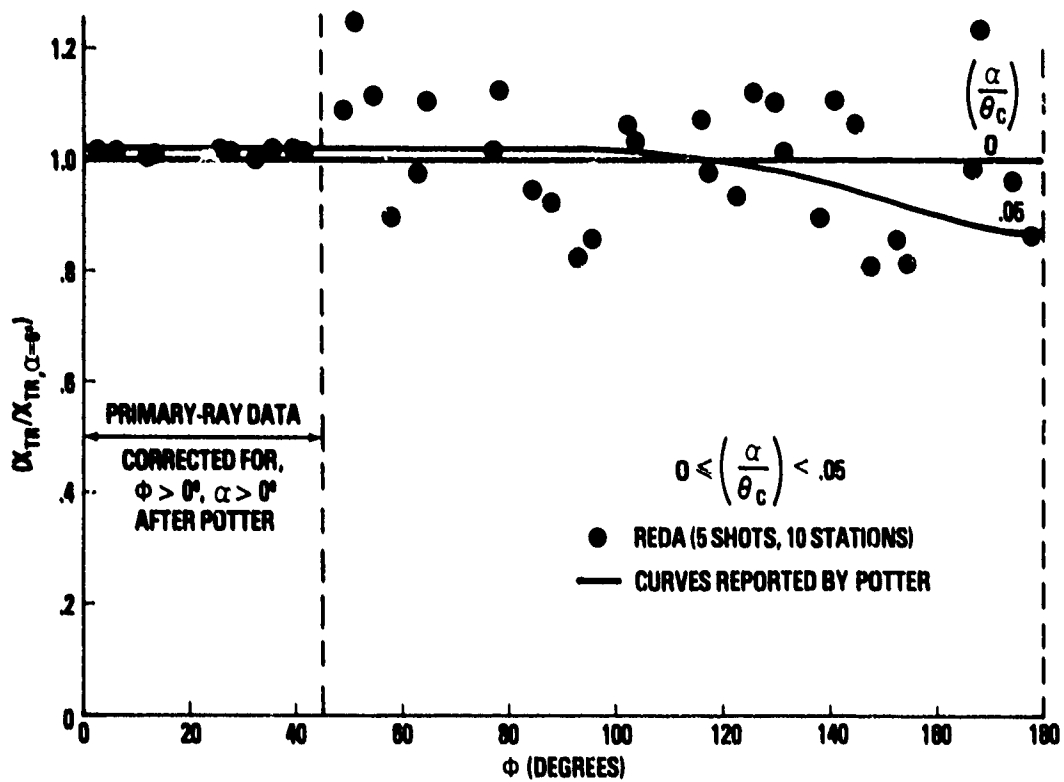


FIGURE 22 TRANSITION ZONE ASYMMETRY; PRESENT DATA VS. POTTER CURVES

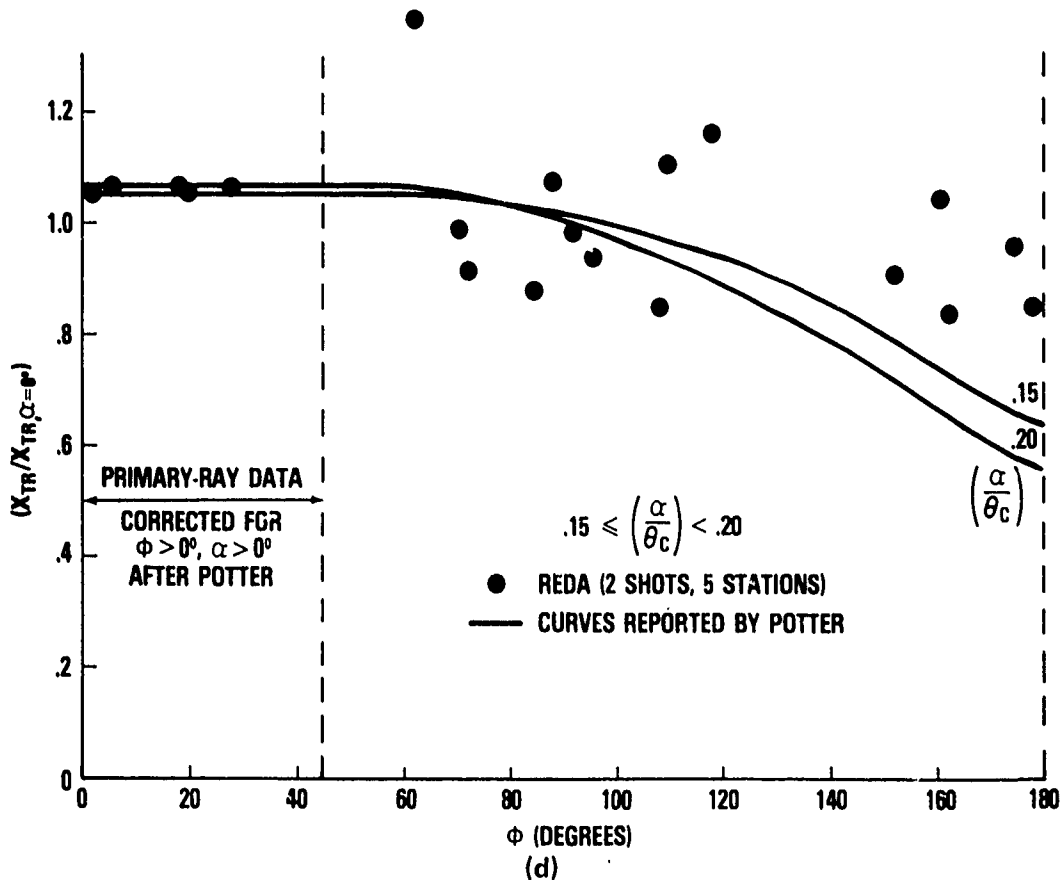
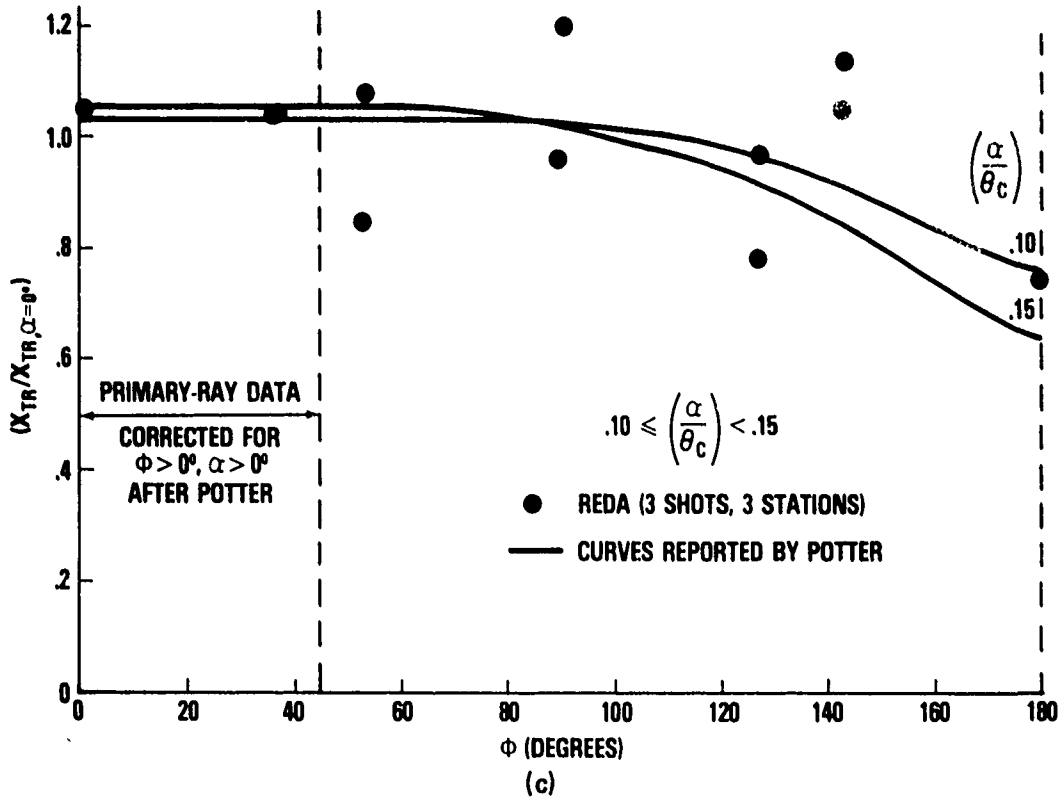


FIGURE 22 TRANSITION ZONE ASYMMETRY; PRESENT DATA VS. POTTER CURVES

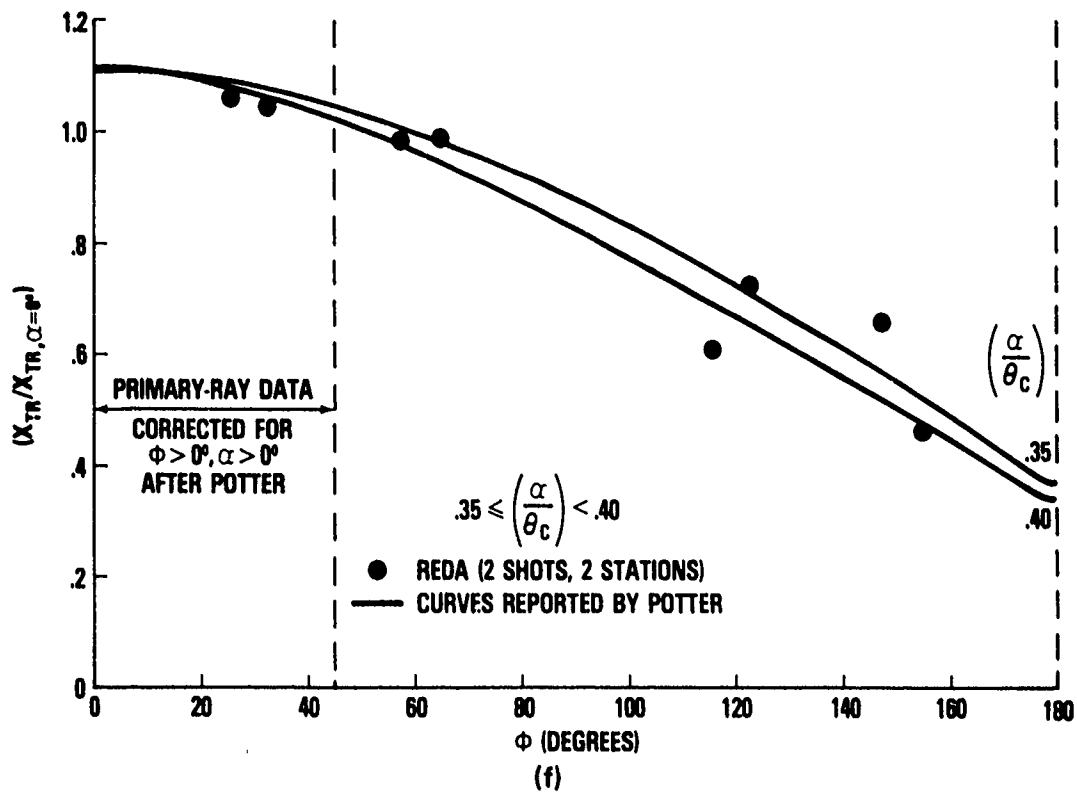
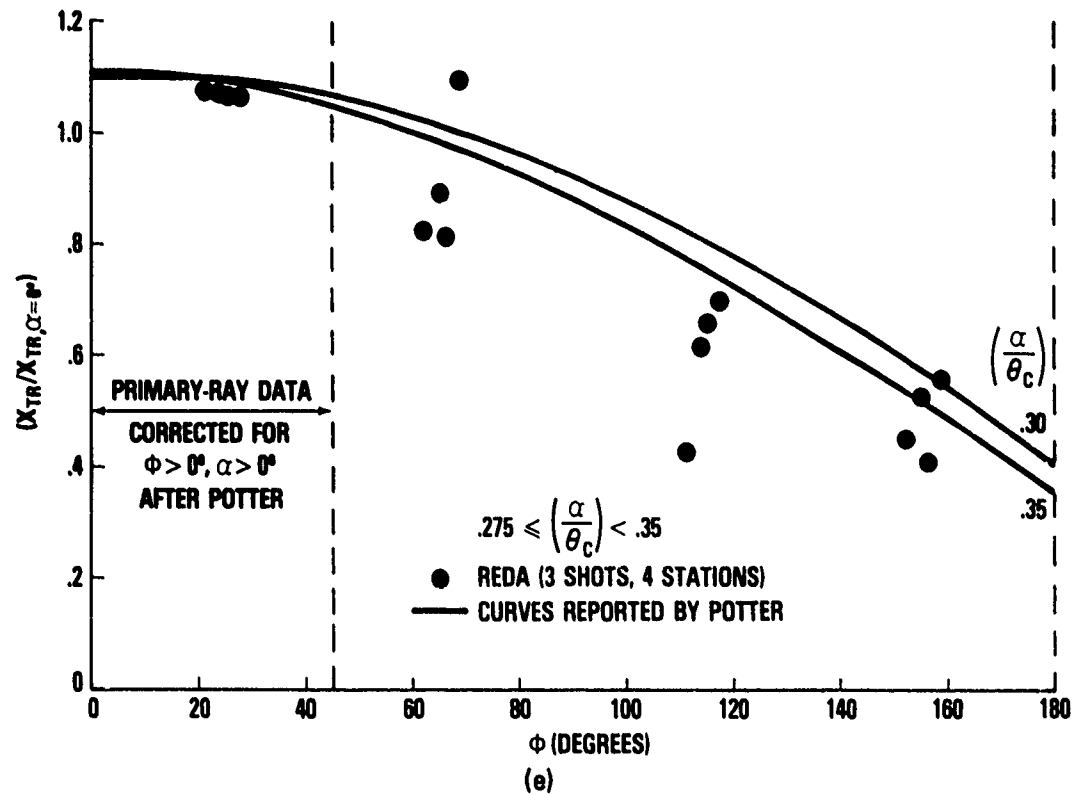


FIGURE 22 TRANSITION ZONE ASYMMETRY; PRESENT DATA VS. POTTER CURVES

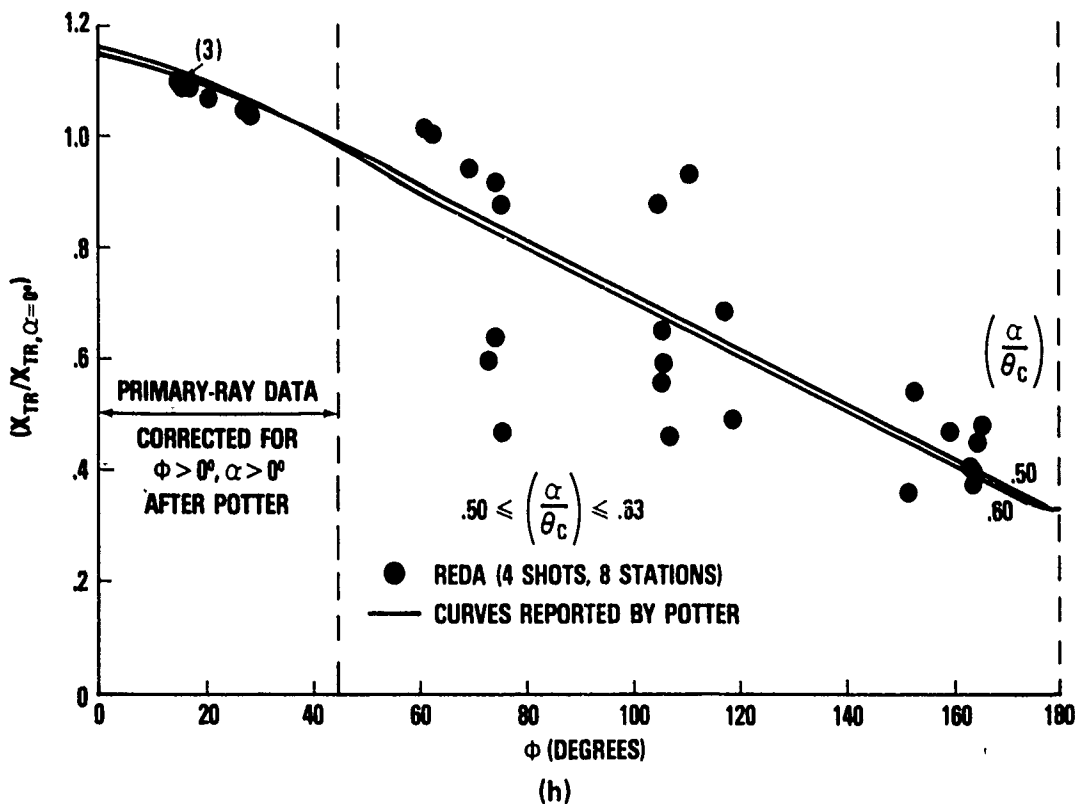
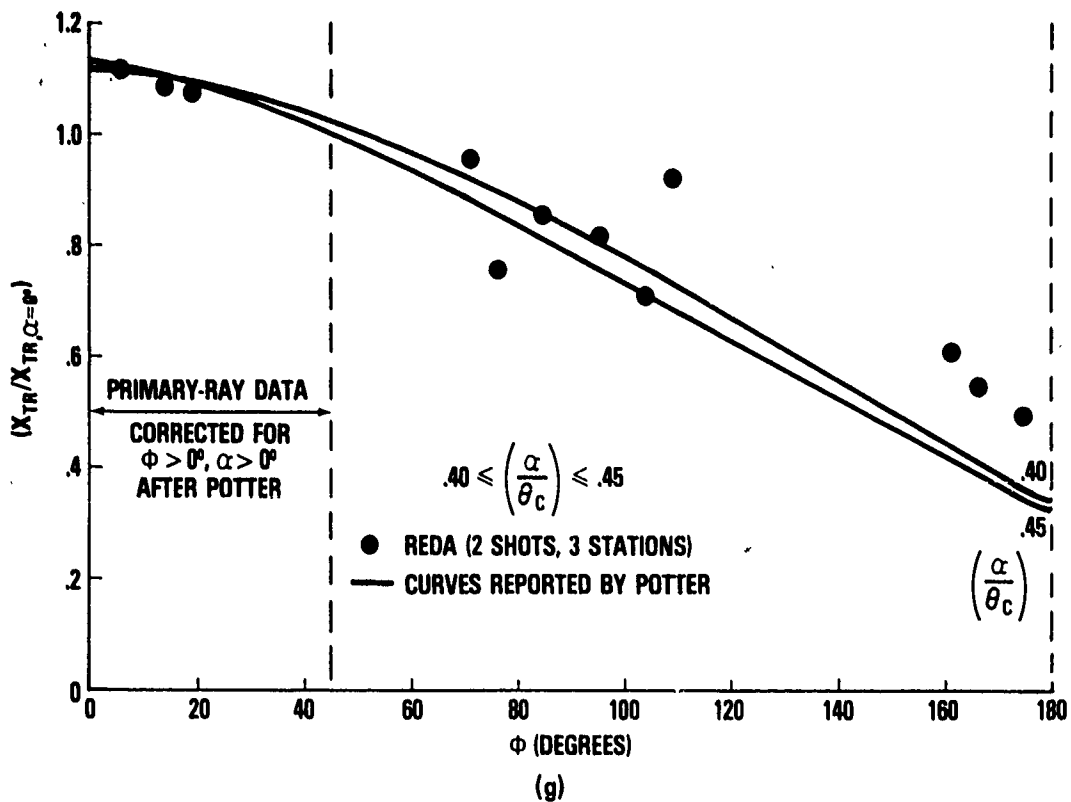


FIGURE 22 TRANSITION ZONE ASYMMETRY; PRESENT DATA VS. POTTER CURVES

AT $\alpha = 0^\circ$

SOURCE	SYM.	TECHNIQUE	FACILITY	θ_c	α/θ_c	M_∞	$\left(\frac{T_w}{T_{aw}}\right)_\theta$	$\frac{U_\theta}{\nu_\theta}, \frac{1}{IN.}$	$\frac{U_\theta^2}{\nu_\theta}, \frac{1}{SEC.}$
REDA	●	DUAL-PLANE SPARK SHADOWGRAPH (5 STATIONS)	RANGE [4 SHOTS]	5.0	.35-.45	4.5	.22-.48	1.04 - 2.66×10^6	0.48 - 1.09×10^{11}
KROGMANN	■	SURFACE HEAT TRANSFER RATES	LUDWIG TUBE	5.0	.35-.45	5.0	—	0.45 - 0.81×10^6	—
KORSIA & MARCILLAT	◇	SINGLE-LINE OILFLOW ("LIMITING STREAMLINES")	TUNNEL	7.5°	.40	5.0	~ 1.0	0.632×10^6	0.22×10^{11}
STETSON & RUSHTON	□	SURFACE HEAT TRANSFER RATES.	SHOCK TUNNEL	8.0	.50	5.5	.24 - .28	~ 0.2 - 0.5×10^6	~ 0.1 - 0.25×10^{11}

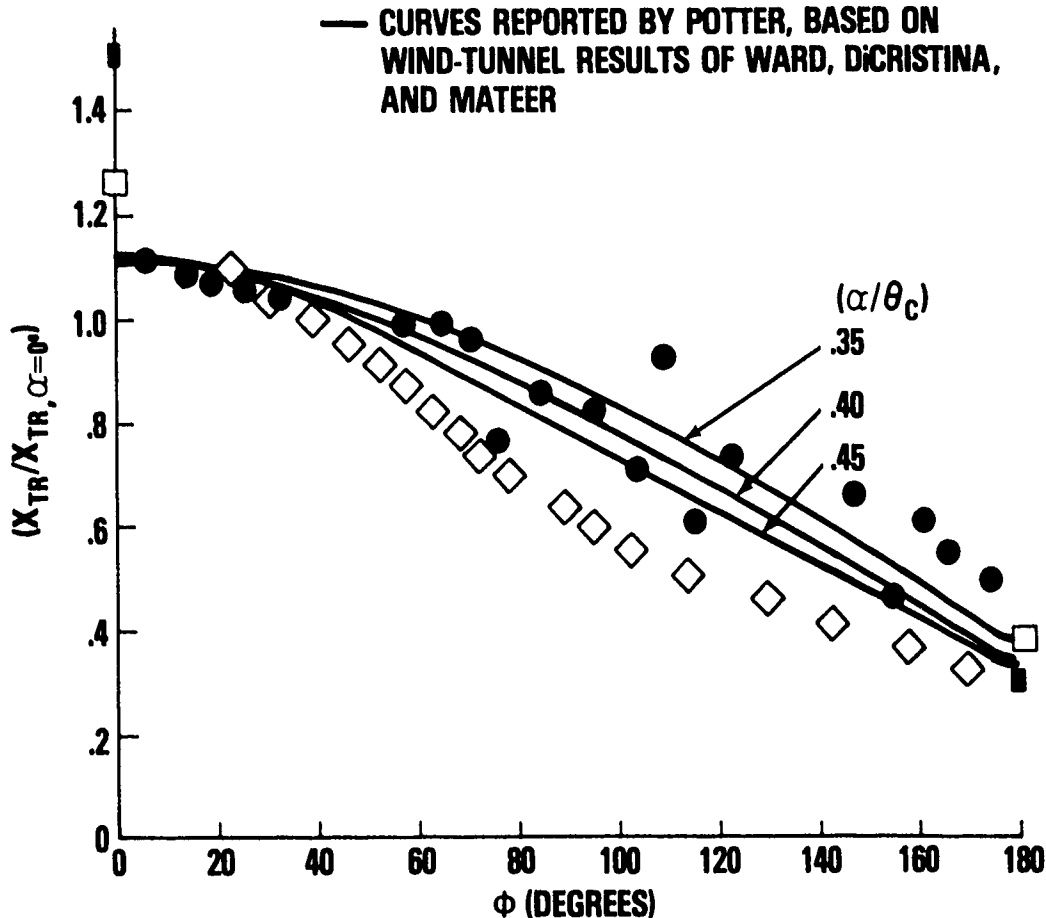


FIGURE 23 TRANSITION ZONE ASYMMETRY; COMPARISONS WITH OTHER MACH FIVE DATA, $.35 \leq (\alpha/\theta_c) \leq .50$

AT $\alpha = 0^\circ$

SOURCE	SYM.	TECHNIQUE	FACILITY	θ_c	α/θ_c	M_∞	$\left(\frac{T_w}{T_{aw}}\right)_e$	$\frac{U_e}{v_e} \cdot \frac{1}{IN.}$	$\frac{U_e^2}{v_e} \cdot \frac{1}{SEC.}$
REDA	●	DUAL-PLANE SPARK SHADOWGRAPH (5 STATIONS)	RANGE [2 SHOTS]	5.0	.15 - .20	4.5	.22 - .35	0.88 - 2.50×10^6	0.43 - 1.53×10^{11}
KROGMANN	■	SURFACE HEAT TRANSFER RATES	LUDWIG TUBE	5.0	.15 - .20	5.0	—	0.45 - 0.81×10^6	—
KORSIA & MARCILLAT	◇	"LIMITING STREAMLINES"	TUNNEL	7.5°	.20	5.0	~ 1.0	0.632×10^6	0.22×10^{11}
	○	SCHLIEREN SURFACE PITOT							
WHITFIELD & DOUGHERTY	▲	SURFACE PITOT	TUNNEL	5.0	.20	4.6	~ 1.0	—	—
STETSON & RUSHTON	□	SURFACE HEAT TRANSFER RATES.	SHOCK TUNNEL	8.0	.25	5.5	.24 - .28	~ 0.2 - 0.5×10^6	~ 0.1 - 0.25×10^{11}

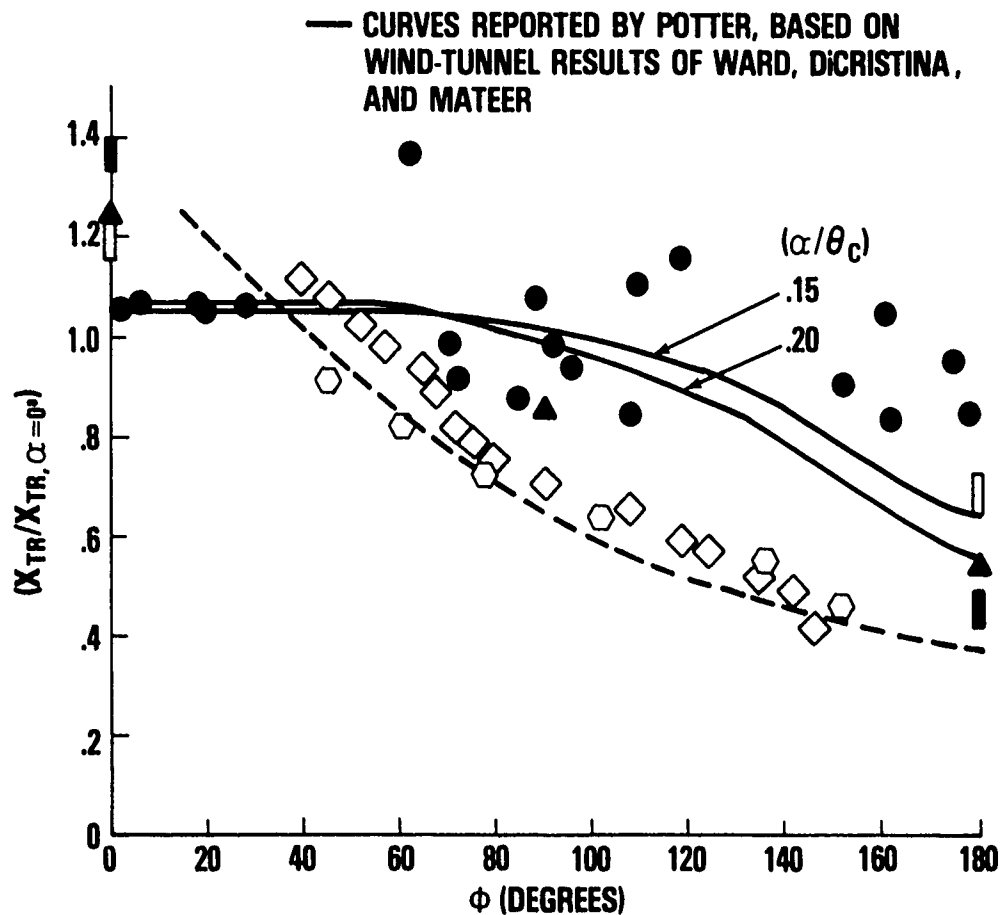


FIGURE 24 TRANSITION ZONE ASYMMETRY; COMPARISONS WITH OTHER MACH FIVE DATA, $.15 < (\alpha/\theta_c) < .25$

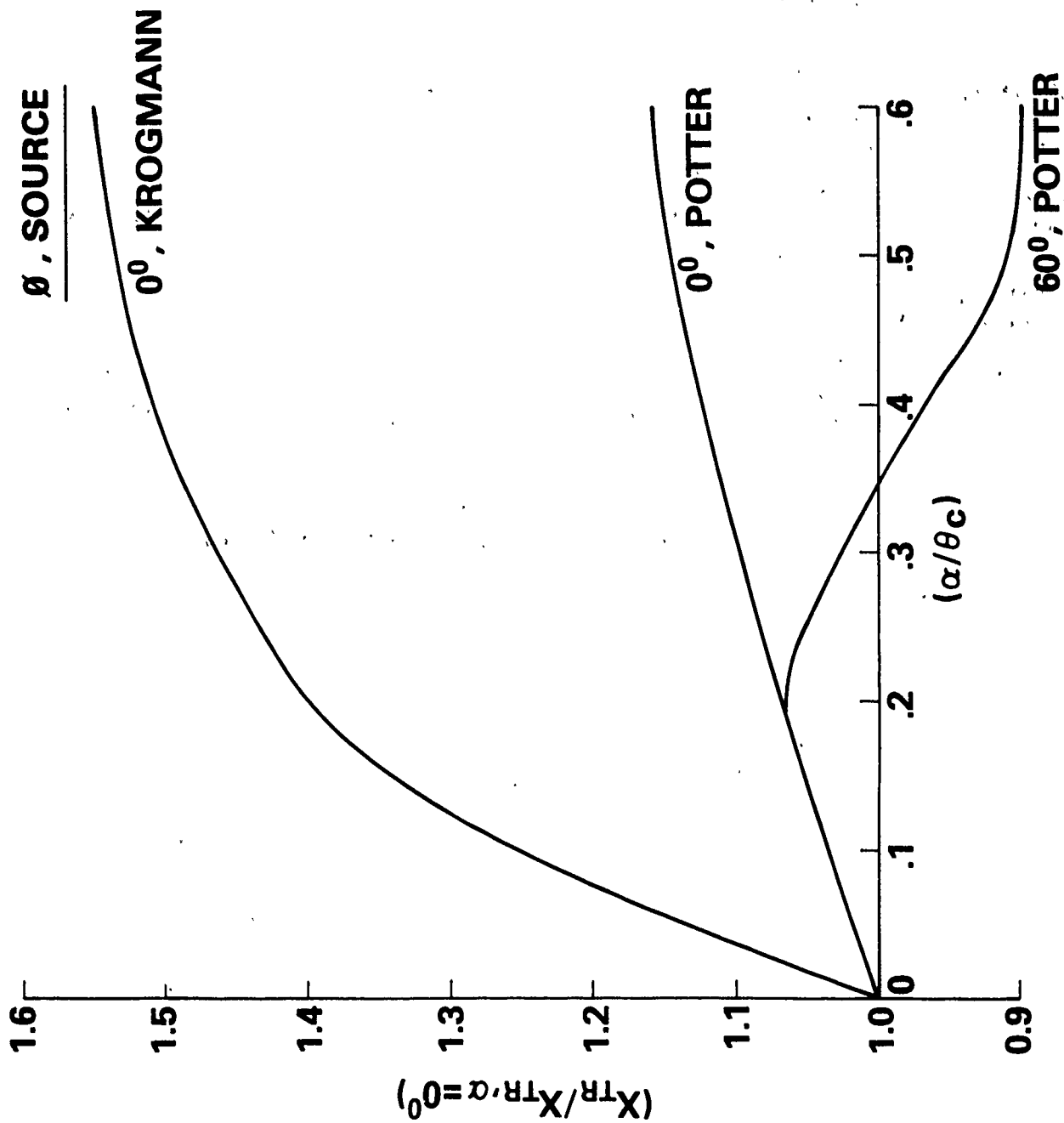


FIGURE 25 TRANSITION ZONE ASYMMETRY DUE TO ANGLE OF ATTACK; POTTER VERSUS KROGMANN

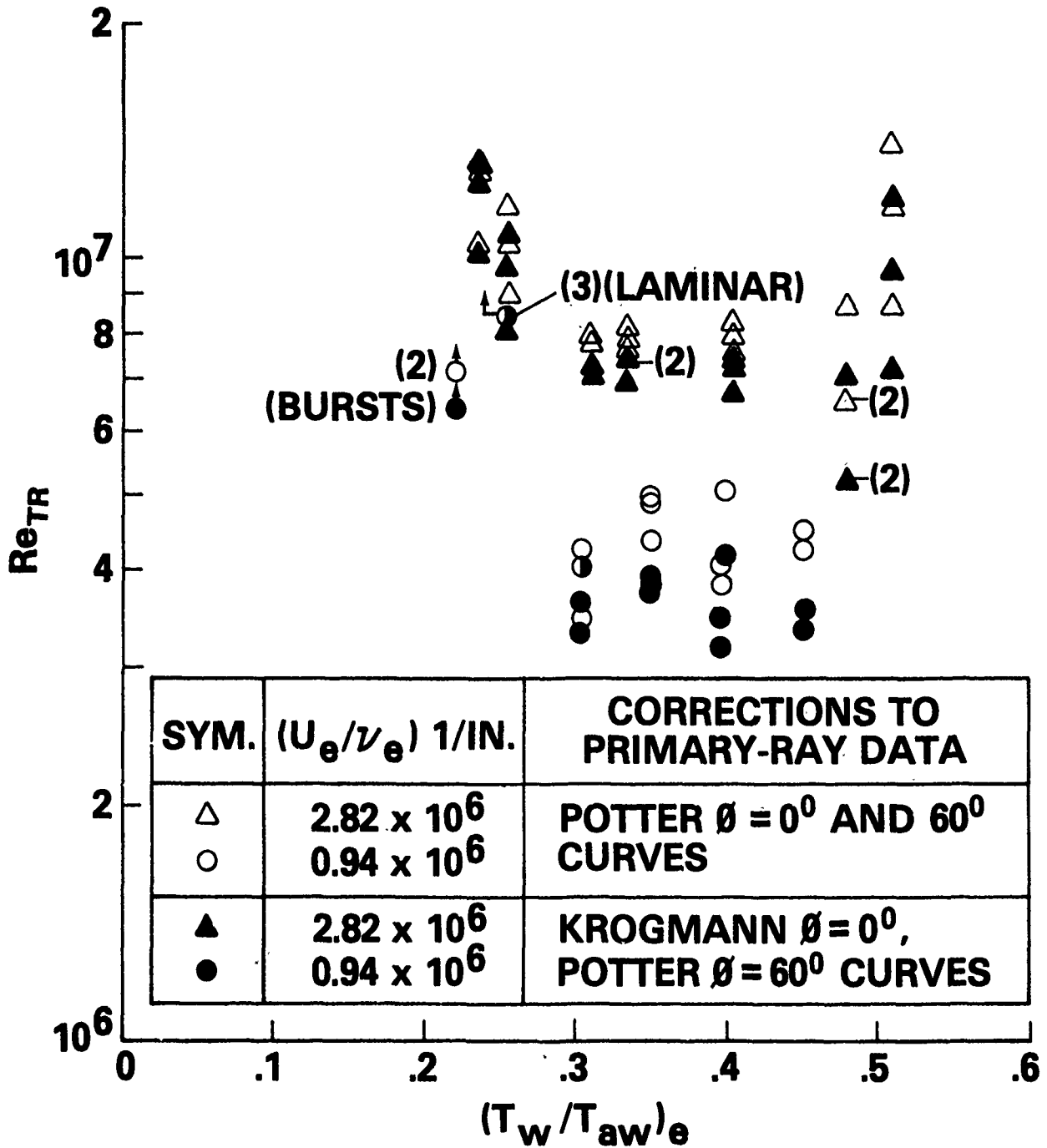


FIGURE 26 TRANSITION REYNOLDS NUMBER VERSUS WALL-TO-ADIABATIC WALL TEMPERATURE RATIO; SENSITIVITY TO CORRECTIONS

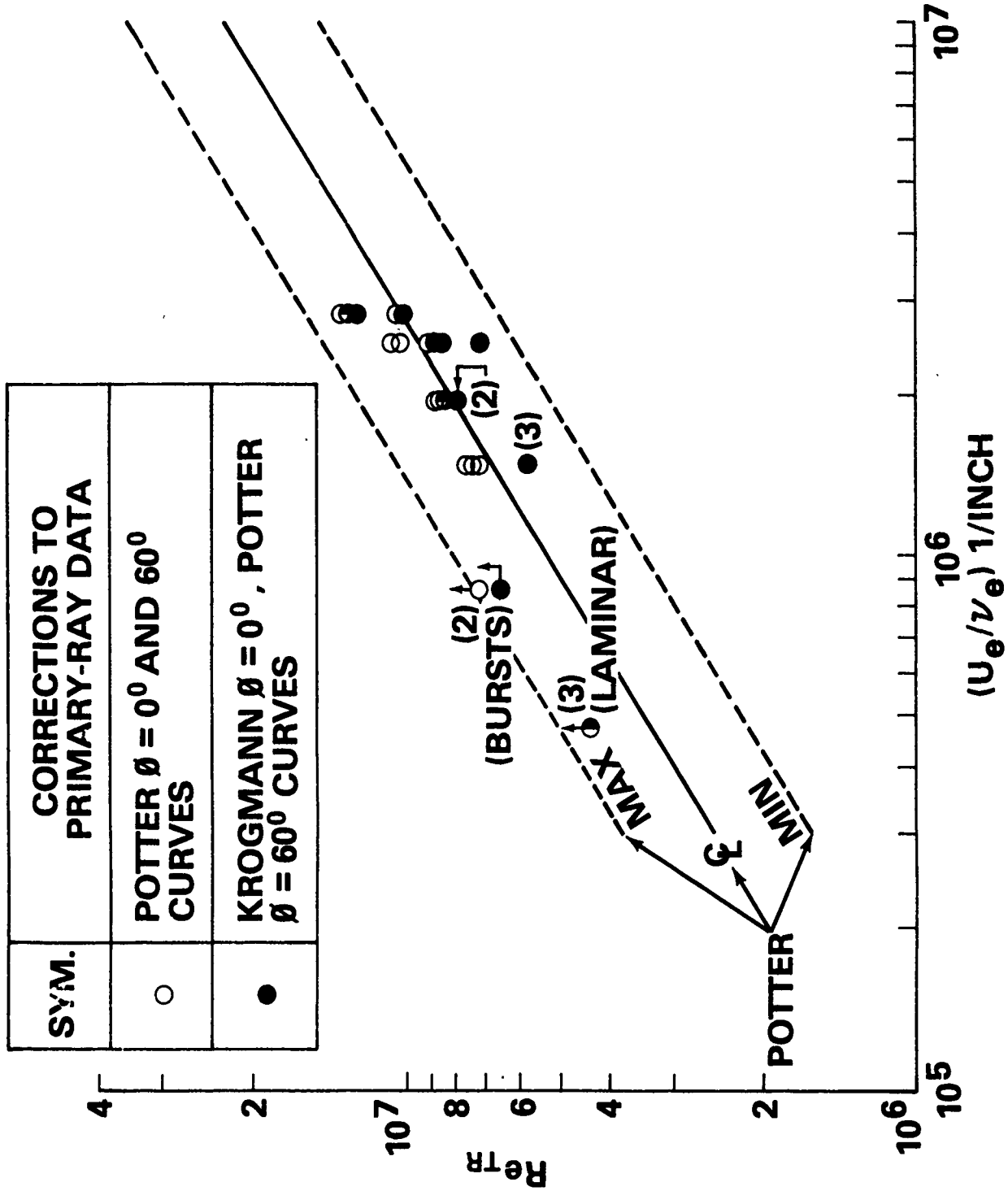


FIGURE 27 TRANSITION REYNOLDS NUMBER VERSUS UNIT REYNOLDS NUMBER; SENSITIVITY TO CORRECTIONS

REFERENCES

1. Pate, S. R. and Schueler, C. J., "Radiated Aerodynamic Noise Effects on Boundary-Layer Transition in Supersonic and Hypersonic Wind Tunnels," AIAA Journal, Vol. 7, No. 3, March 1969, pp. 450-457.
2. Dougherty, N. S., Jr., "Correlation of Transition Reynolds Number with Aerodynamic Noise Levels in a Wind Tunnel at Mach Numbers 2.0 - 3.0," AIAA Journal, Vol. 13, No. 12, Dec 1975, pp. 1670-1671.
3. Tani, I., "Boundary-Layer Transition," Annual Review of Fluid Mechanics, Vol. 1, 1969, pp. 169-196.
4. Morkovin, M. V., "On the Many Faces of Transition," Symposium on Viscous Drag Reduction, LTV Research Center, Dallas, Texas, 24-25 Sept. 1968, pp. 1-31 (Plenum Press, New York, 1969; Library of Congress #77-76496).
5. Morkovin, M. V., "Critical Evaluation of Transition from Laminar to Turbulent Shear Layers with Emphasis on Hypersonically Traveling Bodies," AFFDL-TR-68-149, March 1969.
6. Morkovin, M. V., "Open Questions - Transition to Turbulence at High Speeds, 1971," AFOSR-TR-70-1731, August 1970.
7. Morkovin, M. V., "Instability, Transition to Turbulence and Predictability," Keynote Address to AGARD Symposium on Laminar-Turbulent Transition, Technical University of Denmark, Copenhagen, Denmark, 2-4 May 1977.
8. Reshotko, E., "Boundary-Layer Stability and Transition," Annual Review of Fluid Mechanics, Vol. 8, 1976, pp. 311-349.
9. Reshotko, E., "A Program for Transition Research," AIAA Journal, Vol. 13, No. 3, March 1975, pp. 261-265.
10. Sheetz, N. W., Jr., "Free-Flight Boundary Layer Transition Investigations at Hypersonic Speeds," AIAA Paper No. 65-127, 2nd Aerospace Sciences Meeting, New York, N.Y., Jan. 1965.

NSWC/WOL TR 77-59

11. Sheetz, N. W., Jr., "Boundary-Layer Transition on Cones at Hypersonic Speeds," AIAA Paper No. 67-131, 5th Aerospace Sciences Meeting, New York, N.Y., Jan. 1967.
12. Berger, A.G., Sheetz, N. W., Jr. and Cords, P. H., "Temperature-Control Techniques and Instrumentation for Viscous Flow Investigations in a Ballistics Range," AIAA Paper No. 68-384, 3rd Aerodynamic Testing Conf., San Francisco, CA., April 1968.
13. Sheetz, N. W., Jr., "Ballistics Range Boundary-Layer Transition Measurements on Cones at Hypersonic Speeds," Symposium on Viscous Drag Reduction, LTV Research Center, Dallas, Texas, 24-25 Sept. 1968, pp. 53-83 (Plenum Press, New York, 1969; Library of Congress #77-76496).
14. Sheetz, N. W., Jr., "Ballistics Range Experiments on the Effect of Unit Reynolds Number on Boundary-Layer Transition," Eighth Navy Symposium on Aeroballistics, Naval Weapons Center/Corona Labs, CA., 6-8 May 1969.
15. Potter, J. L., "Observations on the Influence of Ambient Pressure on Boundary-Layer Transition," AIAA Journal, Vol. 6, No. 10, Oct. 1968, pp. 1907-1911.
16. Potter, J. L., "The Unit Reynolds Number Effect on Boundary-Layer Transition," Ph.D. Thesis, Vanderbilt University, May 1974.
17. Potter, J. L., "Boundary-Layer Transition on Supersonic Cones in an Aeroballistic Range," AIAA Journal, Vol. 13, No. 3, March 1975, pp. 270-277.
18. Various Authors, "Ballistics-Range Technology," AGARD-AG-138-70, edited by Canning, T. N., Seiff, A., and James, C. S., Aug. 1970.
19. Laderman, A. J., "Review of Wind-Tunnel Freestream Pressure Fluctuations," AIAA Journal, Vol. 15, No. 4, April 1977, pp. 605-608.
20. Whitfield, J. D. and Dougherty, N. S., Jr., "A Survey of Transition Research at AEDC," AGARD Symposium on Laminar-Turbulent Transition, Technical University of Denmark, Copenhagen, Denmark, 2-4 May 1977 (also published as AEDC-TR-77-52, July 1977).
21. Rhudy, J. P., "Effect of Uncooled Leading Edge on Cooled-Wall Hypersonic Flat-Plate Boundary-Layer Transition," AIAA Journal, Vol. 8, No. 3, March 1970, pp. 576-577.

22. Wilson, R. E., "Laminar Boundary-Layer Growth on Slightly Blunted Cones at Hypersonic Speeds," AIAA Journal of Spacecraft and Rockets, Vol. 2, No. 4, July-Aug., 1965, pp. 490-496.
23. Lyons, W. C., Jr. and Brown, H. S., "The Drag of Slightly Blunted Slender Cones," NOLTR 68-3, Jan. 1968.
24. Lyons, W. C., Jr., "Hypersonic Laminar and Turbulent Heat Transfer for Slightly Blunted Slender Cones," Ph.D. Thesis, University of Maryland, 1969.
25. Stetson, K. F. and Rushton, G. H., "Shock Tunnel Investigation of Boundary-Layer Transition at $M = 5.5$," AIAA Journal, Vol. 5, No. 5, May 1967, pp. 899-906.
26. Rotta, N. R. and Zakkay, V., "Effects of Nose Bluntness on the Boundary Layer Characteristics of Conical Bodies at Hypersonic Speeds," Astronautica Acta, Vol. 13, Nos. 5 and 6, 1968, pp. 507-516.
27. Potter, J. L. and Whitfield, J. D., "Effects of Slight Nose Bluntness and Roughness on Boundary-Layer Transition in Supersonic Flows," Journal of Fluid Mechanics, Vol. 12, No. 4, 1962, pp. 501-535.
28. Murphy, C. H., "Data Reduction for the Free Flight Spark Ranges," Ballistic Research Laboratories, Aberdeen Proving Ground, Md., BRL Report No. 900, Feb. 1954.
29. Ward, L. K., "Influence of Boundary-Layer Transition on Dynamic Stability at Hypersonic Speeds," Transactions of 2nd Technical Workshop on Dynamic Stability Testing, Vol. II, Arnold Engineering Development Center, 1965.
30. DiCristina, V., "Three-Dimensional Laminar Boundary-Layer Transition on a Sharp 8° Cone at Mach 10," AIAA Journal, Vol. 8, No. 5, May 1970, pp. 852-856.
31. Mateer, G. G., "Effects of Wall Cooling and Angle of Attack on Boundary Layer Transition on Sharp Cones at $M_\infty = 7.4$," NASA TN D-6908, 1972.
32. Reda, D. C., "Prepared Comments on Boundary-Layer Transition Research at Supersonic Velocities," AGARD Symposium on Laminar-Turbulent Transition, Technical University of Denmark, Copenhagen, Denmark, 2-4 May 1977.
33. Richards, B. F. and Stollery, J. L., "Further Experiments on Transition Reversal at Hypersonic Speeds," AIAA Journal, Vol. 4, No. 12, Dec. 1966, pp. 2224-2226.

34. Lees, L. and Reshotko, E., "Stability of the Compressible Laminar Boundary Layer," Journal of Fluid Mechanics, Vol. 12, 1962, pp. 555-590.
35. Reshotko, E., "Transition Reversal and Tollmien-Schlichting Instability," The Physics of Fluids, Vol. 6, No. 3, March 1963, pp. 335-342.
36. Mack, L. M., "The Stability of the Compressible Laminar Boundary Layer According to a Direct Numerical Solution," AGARDograph 97, 1965, pp. 483-501.
37. Reshotko, E., "Stability Theory as a Guide to the Evaluation of Transition Data," AIAA Journal, Vol. 7, No. 6, June 1969, pp. 1086-1091.
38. Mack, L. M., "Linear Stability Theory and the Problem of Supersonic Boundary-Layer Transition," AIAA Journal, Vol. 13, No. 3, March 1975, pp. 278-289.
39. Van Driest, E. R. and Blumer, C. B., "Boundary-Layer Transition at Supersonic Speeds: Roughness Effects with Heat Transfer," AIAA Journal, Vol. 6, No. 4, April 1968, pp. 603-607.
40. Van Driest, E. R. and Boison, J. C., "Experiments on Boundary-Layer Transition at Supersonic Speeds," Journal of the Aeronautical Sciences, Vol. 24, No. 12, Dec. 1957, pp. 885-899.
41. Kendall, J. M., "Wind-Tunnel Experiments Relating to Supersonic and Hypersonic Boundary-Layer Transition," AIAA Journal, Vol. 13, No. 3, March 1975, pp. 290-299.
42. Boison, J. C., "Investigation of Test Facility Environmental Factors Affecting Boundary-Layer Transition," AFFDL-TR-73-106, Sept. 1973.
43. Kroghmann, P., "An Experimental Study of Boundary-Layer Transition on a Slender Cone at Mach 5," AGARD Symposium on Laminar-Turbulent Transition, Technical University of Denmark, Copenhagen, Denmark, 2-4 May 1977.
44. Martellucci, A. and Neff, R. S., "Influence of Asymmetric Transition on Re-entry Vehicle Characteristics," AIAA Journal of Spacecraft and Rockets, Vol. 8, No. 5, May 1971, pp. 476-482.
45. Chrusciel, G. T., "Analysis of Re-entry Vehicle Behavior during Boundary-Layer Transition," AIAA Journal, Vol. 13, No. 2, Feb. 1975, pp. 154-159.

46. Liepman, H. P., "Analysis of Boundary Layer Transition Effects on Ballistic Reentry Vehicle Impact Dispersion and Comparison with Other Dispersion Factors," Institute for Defense Analysis, Paper P-1137, December 1975.
47. Korsia, A. and Marcillat, J. F., "Three-Dimensional Boundary-Layer Transition on a Yawed 7.5° Sharp Cone at $M = 5$," AGARD Symposium on Laminar-Turbulent Transition, Technical University of Denmark, Copenhagen, Denmark, 2-4 May 1977.

LIST OF SYMBOLS

c	speed of sound
CP_N, CG_N	non-dimensional center of pressure, gravity, measured from cone tip
L_c	cone length
M	Mach number
n	exponent of unit Reynolds number
p	pressure
\tilde{p}	fluctuating pressure
Re_{TR}	transition Reynolds number, $\frac{\rho_e U_e X_{TR}}{\mu_e}$
Re_L	cone-length Reynolds number, $\frac{\rho_e U_e L_c}{\mu_e}$
$Re_{N,t}$	nose-radius Reynolds number, $\frac{\rho_t c_t R_N}{\mu_t}$
R_N	nosetip radius
r	recovery factor
S	arc length along surface, measured from stag. point
\bar{S}	non-dimensional arc length, defined by eq. (3)
S.M.	static margin = $CP_N - CG_N$
T	temperature
ΔT	temperature change
t	time

U	velocity
X_{TR}	transition run length
X	range horizontal coordinate
Y	range vertical coordinate
α	angle of attack
γ	ratio of specific heats
θ_c	cone half-angle
μ	viscosity
ν	kinematic viscosity, μ/ρ
ρ	density
ϕ	circumferential angle, measured from windward ray
ϕ'	angle defined by eq. (6)

Subscripts

aw	adiabatic wall
e	at edge of boundary layer, or based on edge properties
H	in "horizontal" plane
i	initial
lee	on leeward side
t	based on stagnation-point properties
V	in "vertical" plane
w	at wall, or based on wall properties
wind	on windward side
$\alpha = 0^\circ$	at zero angle of attack
∞	freestream